Chemical Engineering Research and Design 234 (2026) 217–237

Contents lists available at ScienceDirect

Chemical Engineering Research and Design

journal homepage: www.elsevier.com/locate/cherd

Pulse-jet regeneration of surface filters at low absolute pressures

Vanessa Löschner *, Patricia Heuer, Jörg Meyer, Achim Dittler

KIT, Institute of Mechanical Process Engineering and Mechanics (MVM) – Research Group Gas Particle Systems, Straße am Forum 8, 76131, Karlsruhe, Germany

ARTICLE INFO

Keywords:
Surface filtration
Filter regeneration
Pulse-jet cleaning
Low pressure applications

ABSTRACT

Pulse-jet cleaning of surface filters at reduced absolute pressure is not yet well quantified. This work investigates pulse-jet regeneration at $p_{\mathrm{abs}} = 900$, 100, 25, and 10 hPa using a flexible spunbond (SB) medium and a rigid sintered granular medium (SG). Regeneration pulses were first characterized on clean media while varying valve opening time, tank pressure, absolute pressure and filter face velocity. The valve opening time primarily controlled pulse duration, whereas variation of tank pressure mainly affected the maximum differential pressure. At constant tank pressure and valve opening time, decreasing absolute pressure increased the maximum differential pressure and delayed the occurrence of this maximum. For comparable cleaning strengths across all absolute pressures, tank pressure was adjusted at each absolute pressure to approach a predefined target value of the maximum differential pressure. Filter cakes were formed using Mikhart MU 08 at similar mass loadings of approximately $50\,\mathrm{g\,m^{-2}}$. High-speed imaging synchronized with the differential pressure signal reveals distinct medium dependent detachment dynamics. For SB, cake detachment starts close to flow reversal, whereas for SG detachment is delayed. Reduced absolute pressure shifts the timing and prolongs the duration of the cake detachment phase. Cleaning efficiencies decrease with decreasing absolute pressure for comparable pulse strengths, with a stronger sensitivity for SG than for SB.

1. Introduction

In many industrial processes, particulate matter must be removed from gas streams in order to comply with emission limits, recover valuable product, or protect downstream equipment from fouling (Wines and Mokhatab, 2022; Hasler and Nussbaumer, 1999; Brown, 2001; Amjad, 2022). This is e.g. also highly relevant for vacuum drying processes, where vapor leaving the drying chamber can entrain fine product particles (Van'T Land, 2011; Jousten, 2018). In industrial vacuum dryers, surface filters are therefore commonly installed to clean the exhaust gas, enable product recovery, and protect subsequent components such as compressors and condensers from contamination (Thier, 1997; Jorisch, 1999). Surface filters are particularly suitable for such applications because they can achieve high separation efficiencies already at the beginning of operation (depending on the filter medium) and can be regenerated effectively (Löffler, 1988; Schmidt, 1998; Beuth Verlag, 2010). A well established industrial method for filter cake detachment and regeneration is pulse-jet cleaning. In this method, a short, defined pressure pulse is introduced through a blow tube into the clean gas side of the filter element. The resulting rise in absolute pressure on the clean side can exceed the absolute pressure on the raw gas side, causing a temporary flow reversal through the filter medium. If the forces induced by the pulse exceed the adhesion forces between the filter cake and the filter medium, the cake detaches from the filter surface (Löffler, 1988; Schmidt, 1998; Verein Deutscher Ingenieure e.V., 2014; Löffler et al., 1984).

During filtration and regeneration the differential pressure across the filter element is typically the experimentally accessible quantity. For a loaded surface filter, it is convenient to split the total differential pressure into contributions of the clean filter medium and the filter cake (Löffler, 1988),

$$\Delta p_{\mathrm{Tot}} = \Delta p_{\mathrm{FM}} + \Delta p_{\mathrm{FC}}. \tag{1}$$

When laminar flow in the continuum regime are assumed, both contributions can be described by linear resistance relations that scale with the gas viscosity μ and the filter face velocity v_F (defined as $v_F = \dot{V}/A_F$, with volumetric flow rate $\dot{V}$ and filtration area A_F). A commonly used representation is

$$\Delta p_{\mathrm{FM}} = K_1\,\mu\,v_F, \tag{2}$$

for the unloaded medium and

$$\Delta p_{\mathrm{FC}} = K_2\,\mu\,v_F\,W, \tag{3}$$

for the filter cake, where K_1 denotes the medium resistance coefficient, K_2 the filter cake resistance and $W = m_{\mathrm{FC}}/A_F$ the cake mass loading with cake mass m_{FC} (Löffler, 1988).

* Corresponding author.
E-mail address: vanessa.loeschner@kit.edu (V. Löschner).

https://doi.org/10.1016/j.cherd.2026.08.058
Received 25 April 2026; Received in revised form 31 July 2026; Accepted 29 August 2026
Available online 8 September 2026

Regeneration performance can be quantified by a cleaning efficiency based on optical, gravimetric or differential pressure measurements. An optical cleaning efficiency is defined as the optically detected fraction of cleaned filter surface

$$E_{\text{opt}} = \frac{A_{\text{FC}} - A_{\text{FC,res}}}{A_{\text{FC}}}, \quad (4)$$

where A_{FC} is the filter cake area before regeneration and $A_{\text{FC,res}}$ is the remaining cake-covered area after regeneration. Likewise, a gravimetric cleaning efficiency can be defined as

$$E_{\text{grav}} = \frac{m_{\text{FC}} - m_{\text{FC,res}}}{m_{\text{FC}}}, \quad (5)$$

where m_{FC} is the cake mass before regeneration and $m_{\text{FC,res}}$ is the remaining filter cake mass after regeneration. Analogously, a differential pressure based cleaning efficiency is defined from the residual cake differential pressure after the pulse relative to the value before regeneration,

$$E_{\Delta p} = \frac{\Delta p_{\text{FC}} - \Delta p_{\text{FC,res}}}{\Delta p_{\text{FC}}}, \quad (6)$$

where Δp_{FC} is the cake differential pressure before regeneration and $\Delta p_{\text{FC,res}}$ is the residual cake differential pressure after regeneration. With these definitions, ideal regeneration yields $E_{\text{opt}} = E_{\text{grav}} = E_{\Delta p} = 1$, whereas incomplete regeneration results in $E_X < 1$.

In practice, $E_X < 1$ is common and can arise from incomplete cake removal during the pulse, e.g. non uniform detachment (patchy cleaning), i.e., locally remaining filter cake patches after regeneration, which is often promoted by very thin filter cakes (Dittler, 2001). Incomplete regeneration can also be associated with dust penetration into the filter medium, where particles deposited within the pore space are not fully expelled during the pulse. Since E_{opt}, E_{grav} and $E_{\Delta p}$ are based on the cleaned area, the removed mass and the residual differential pressure, respectively, they need not be identical. These differences are discussed together with the results in Section 3.2.3. In this context it should be noted that the residual differential pressure, on which $E_{\Delta p}$ is based, may be nearly independent of E_X under certain conditions (Dittler, 2001).

Pulse-jet cleaning of surface filters at ambient absolute pressure has been studied extensively, including investigations of flat media (circular samples), filter bags, and cartridge filters (Yu et al., 2024; Liu and Shen, 2019; Sievert and Löffler, 1989; Leubner and Riebel, 2003; Rothwell, 1991a; Bächler et al., 2023, 2026; Klingel and Löffler, 1984; Krammer and Holzinger, 2022; Kurtz et al., 2016; Silva et al., 1999). It has been shown that regeneration success cannot be explained by a single pulse parameter alone (Leubner and Riebel, 2004), although some studies focus primarily on maximum pulse values (Sievert and Löffler, 1989). A pressure pulse can be quantified using different metrics, for example the maximum differential pressure during regeneration, $\Delta p_{\text{max,Reg}}$, the maximum differential pressure rise rate, $(\mathrm{d}\Delta p/\mathrm{d}t)_{\text{max}}$, or the differential pressure integral, $\int \Delta p\, \mathrm{d}t$. In addition, the pulse shape is often described qualitatively in terms of the *pulse strength*, which is frequently associated with a higher $\Delta p_{\text{max,Reg}}$. For a given regeneration setup, a higher $\Delta p_{\text{max,Reg}}$ typically coincides with a higher maximum rise rate $(\mathrm{d}\Delta p/\mathrm{d}t)_{\text{max}}$ and a larger differential pressure time integral $\int \Delta p\, \mathrm{d}t$. However, these relations depend on the pulse shape and duration and are therefore not universal.

For flat media, regeneration performance depends strongly on tank pressure and on the specific geometry of the regeneration system, including blow tube diameter and the distance between blow tube and filter medium (Krammer and Holzinger, 2022; Verein Deutscher Ingenieure e.V., 2014; Schuberth et al., 2011; Bächler et al., 2026; Binnig et al., 2011). Literature further reports that increasing tank pressure leads to higher pulse strength and that both the pressure rise rate $\mathrm{d}p/\mathrm{d}t$ and the pressure integral increase approximately linearly with tank pressure (Leubner and Riebel, 2003; Simon et al., 2007). Moreover, the transient pressure pulse can exhibit superimposed fluctuations whose structure depends on the injector system and the measurement location (Rothwell, 1991a; Leubner and Riebel, 2003). Pulse strength is often reported using the maximum absolute pressure on the clean gas side, p_{max}, whereas many experimental setups evaluate the maximum differential pressure across the filter, $\Delta p_{\text{max,Reg}}$. In this work, $\Delta p_{\text{max,Reg}}$ is used; the reasons are given in Section 2.4.5.

Notably, the governing regeneration mechanisms are strongly influenced by the mechanical properties of the filter medium (e.g. thickness, rigidity, pores diameter, ...). Flexible media (e.g., needle felts or spunbond media) can deform and inflate during the pulse. This deformation may enhance regeneration because an additional impulse is introduced via the acceleration and subsequent deceleration of the filter medium (Krammer and Holzinger, 2022). In contrast, rigid media such as sintered metal filters or sintered porous polymer filter media do not significantly deform. In these cases, filter cake detachment is mainly driven by flow reversal and the transient differential pressure acting across the filter cake. Consequently, higher pulse strengths are typically required for rigid media to achieve cleaning performances comparable to flexible media, because deformation induced impulses are absent (Löffler et al., 1984; Beuth Verlag, 2010).

While pulse-jet regeneration of surface filters is well understood at ambient conditions, the influence of reduced absolute pressure on regeneration performance has not yet been investigated systematically. Nevertheless, a change in regeneration behavior is expected at lower absolute pressure because gas density, jet momentum, and pressure-wave propagation differ from ambient conditions. At reduced absolute pressure, previous work has focused on the differential pressure behavior of unloaded filter media (including modeling) and on filter cake build-up and resulting differential pressure as a function of absolute pressure (Löschner et al., 2025, 2026a). These studies indicate that the differential pressure decrease with reduced absolute pressure. The filter cake structure and thus its permeability appears to be largely independent of whether the filter cake is formed at ambient or at reduced absolute pressure. Whereas the spatial filter cake distribution on the filter medium becomes less homogeneous as absolute pressure decreases. In addition, a specific filter cake constant K_{FC} (defined analogously to K_2') was reported to be nearly identical for a given absolute pressure, regardless of whether the filter cake was formed at that specific reduced absolute pressure or formed at ambient pressure followed by absolute pressure reduction.

In this paper, pulse-jet regeneration of surface filter media at reduced absolute pressures ($p_{\text{abs}} = 900,\ 100,\ 25,\ 10\,\text{hPa}$) is investigated. First, the pressure pulses of two different unloaded filter media are analyzed to characterize the pulse shape and its dependence on p_{abs} for a defined geometry of the regeneration system, including the role of valve opening time and tank pressure in determining the attainable maximum differential pressure for different media. This characterization is used to define target regeneration parameters for the subsequent filter cake detachment experiments and to ensure comparability between operating pressures by adjusting the tank pressure to reach consistent levels of $\Delta p_{Reg,\text{max}}$. Subsequently, regeneration experiments on loaded filter media are conducted at the same operating pressures. To ensure comparable initial conditions, the filter cakes are generated under identical loading conditions at $p_{\text{abs}} = 900\,\text{hPa}$, yielding a similar mass loading W on both media prior to regeneration. Regeneration performance is assessed using the optical, gravimetric and differential pressure based cleaning efficiencies, E_{opt}, E_{grav} and $E_{\Delta p}$ (Eqs. (4) – (6)). In addition, each pulse is recorded at high temporal resolution and analyzed in terms of the maximum pulse differential pressure $\Delta p_{Reg,\text{max}}$ and the maximum differential pressure rise rate $\left(\mathrm{d}\Delta p_{\text{Reg}}/\mathrm{d}t\right)_{\text{max}}$.

2. Materials and methods

2.1. Experimental set-up

A schematic diagram of the experimental set-up is presented in Fig. 1. The experimental set-up consists of three functional segments: the

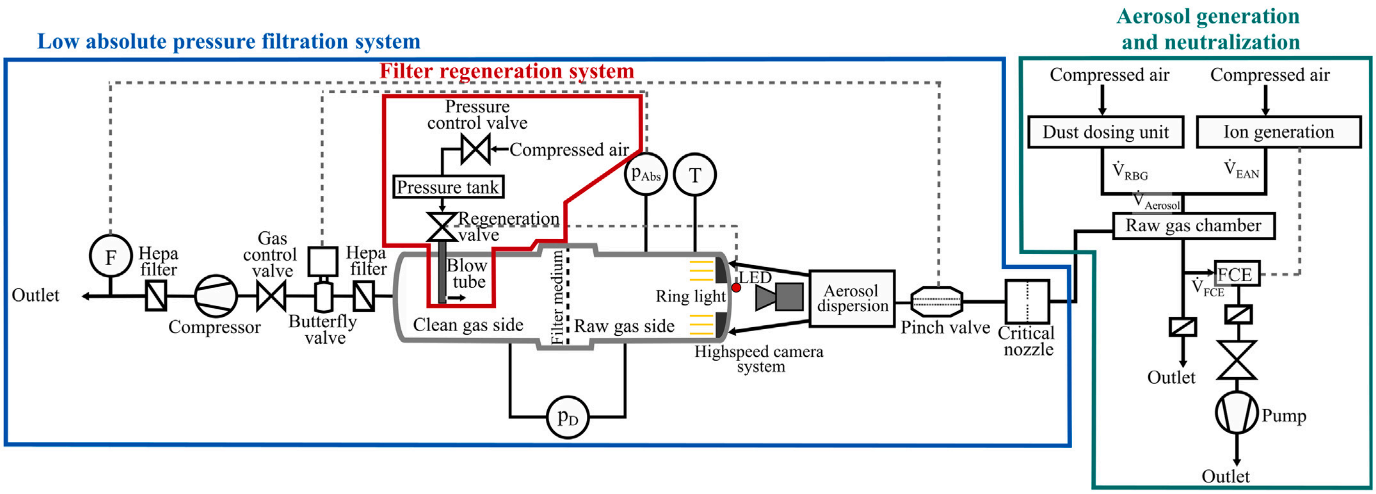

Fig. 1. Schematic overview of the experimental setup.

low absolute pressure filtration system (labeled in blue), the aerosol generation and neutralization unit (labeled in green) and the key unit of this work the filter regeneration system (labeled in red). To provide a comprehensive overview, the individual components are explained in more detail in the following sections.

2.1.1. Low absolute pressure filter system

The main component of the experimental setup consists of the filter chamber and the associated flow and absolute pressure regulation system highlighted in blue in Fig. 1. On the raw gas side, the aerosol laden gas enters the chamber through four inlets and is assumed to distribute uniformly across the filter chamber cross section. A central optical access port is positioned at the corresponding side of the filter chamber in the form of a 6 cm diameter glass window, which enables access for high speed imaging of the filter surface during regeneration.

The inlet volumetric flow rate $\dot{V}_{\mathrm{Aerosol}}$ is pre-set using one of two inlet nozzles (IN), selected according to the desired flow range. A nozzle with a diameter of $d_{\mathrm{IN,1}} = 2.94\,\mathrm{mm}$ is used for operating volumetric flow rates up to $46\,\mathrm{L\,min^{-1}}$, whereas a nozzle with $d_{\mathrm{IN,2}} = 1.36\,\mathrm{mm}$ is used for low flow operation below $10\,\mathrm{L\,min^{-1}}$. Fine adjustment of the flow rate is achieved with an additional pinch valve (KVT GmbH, DN 6) in series. Circular filter samples with a free filtration area of $154\,\mathrm{cm^2}$ are clamped into a filter medium holder and are installed 53 cm downstream of the inlet region. A HEPA filter is installed downstream on the clean gas side to protect subsequent components from particle contamination. The raw gas side absolute pressure is controlled using a gas control valve (EVR 116, Pfeiffer Vacuum GmbH, ISO KF DN 16) in series with a butterfly valve (VAT Group AG, ISO KF DN 25). The flow rate is measured on the clean gas side downstream of the compressor using thermal mass flow meters (MFM) (MKS Instruments Deutschland GmbH). Two MFMs with full scale ranges of $50\,\mathrm{L\,min^{-1}}$ and $2\,\mathrm{L\,min^{-1}}$ are used (specified at normal temperature and pressure (NTP)), each with a resolution of 0.1 % of full scale. Together with the prevailing raw gas side operating pressure, these measurements are used to determine the actual volumetric flow through the system at operating condition and thus, the filter face velocity v_F.

The raw gas temperature is measured using a Pt100 sensor. The raw gas absolute pressure is monitored with a Pirani vacuum transmitter (Thyracont Vacuum Instruments GmbH) covering a measurement range from $5 \cdot 10^{-5}\,\mathrm{mbar}$ to 2000 mbar. The specified accuracy is < 2 % of reading for 200 mbar to 2000 mbar, < 5 % of reading for 40 mbar to 200 mbar, and < 10 % of reading for $2 \cdot 10^{-3}\,\mathrm{mbar}$ to 40 mbar. The differential pressure across the filter medium is measured using three different sensors. Two differential pressure transmitters (IPD 40, ICS Schneider Messtechnik GmbH) are used for continuous monitoring during filtration and are recorded with a temporal resolution of 1 s. Their measuring ranges are 0 mbar to 50 mbar and 0 mbar to 200 mbar, respectively, with a specified accuracy of ≤ ±0.2 % of full scale. A third differential pressure sensor is used only during regeneration in order to capture the transient pressure pulse with high time resolution. This sensor covers a range from 0 mbar to 100 mbar, has a specified accuracy of ±0.1 % of full scale and records the signal with one millisecond resolution during the pulse event. Since the differential pressure is measured from the low pressure side to the high pressure side during regeneration, this sensor resolves negative values only down to approximately −8 hPa.

In this study, the volumetric flow rate is adjusted such that a constant filter face velocity of either $v_F = 5.5\,\mathrm{cm\,s^{-1}}$ or $v_F = 2.0\,\mathrm{cm\,s^{-1}}$ is maintained at the respective system pressure. For operation near ambient pressure it should be noted that, at the applied filter face velocities, a raw gas side pressure of $10^5\,\mathrm{Pa}$ cannot be reached due to the pressure losses across the inlet nozzle and the pinch valve. Moreover, the achievable raw gas side pressure under nominally ambient operation depends on the atmospheric pressure on the day of measurement. Averaging over tests performed on different days yielded a mean raw gas side absolute pressure of approximately 900 hPa. Accordingly, $p_{\mathrm{abs}} = 900\,\mathrm{hPa}$ is used throughout this work to represent ambient absolute pressure.

2.1.2. Aerosol generation and neutralization

The aerosol generation and neutralization system is shown in green in Fig. 1. The aerosol for filter cake build up is produced using a rotating brush generator (RBG 900, Palas GmbH) operated at a constant inlet pressure of 1.4 bar, corresponding to a volumetric flow of $\dot{V}_{\mathrm{RBG}} = 53\,\mathrm{L\,min^{-1}}$. The feed rate can be adjusted over a wide range to set the targeted raw gas concentration. Downstream, the aerosol is neutralized using an aerosol neutralizer (EAN 581, Topas GmbH), and the aerosol charge is assessed using a Faraday cup electrometer (FCE; ACD 331, Topas GmbH). Since the aerosol is predominantly positively charged, only the negative ion head is operated. The neutralization procedure and the setup are described in detail in Löschner et al. (2026a). The combined volumetric flow of generator and neutralizer amounts to $\dot{V}_{\mathrm{Aerosol}} = 98\,\mathrm{L\,min^{-1}}$. Downstream, the aerosol enters a raw gas mixing chamber to increase residence time and to obtain a more stable raw gas concentration. Depending on the selected absolute pressure and filter face velocity, part of the flow is directed to the filter chamber, while the excess flow is discharged to the environment through exhaust filters. From the excess stream, a sampling flow of $\dot{V}_{\mathrm{FCE}} = 3.33\,\mathrm{L\,min^{-1}}$ is taken for the FCE and set using a rotameter.

2.1.3. Filter medium regeneration system

The filter medium regeneration system is the key component for the filter cake detachment experiments. It is highlighted in red in Fig. 1

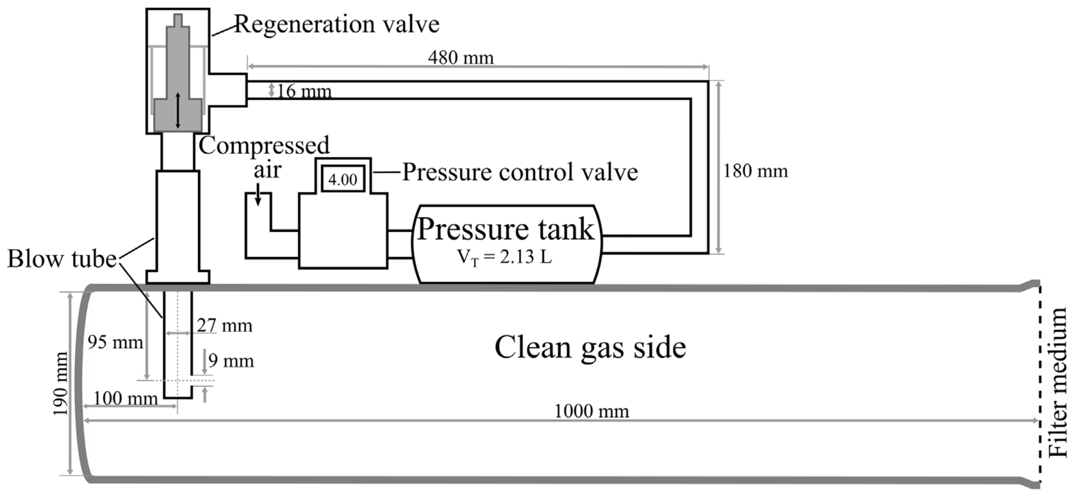

Fig. 2. Detailed schematic overview of the filter medium regeneration system.

and a detailed schematic is shown in Fig. 2. Absolute pressure in the pressure tank is set using a pressure control valve connected to the compressed air line. The geometric tank volume is 2 L, including the piping up to the regeneration valve, an effective tank volume of 2.13 L is obtained. In this work, all tank pressures are reported as absolute values to remain consistent with the other pressure quantities given also as absolute pressures.

The pressure pulse is released by a fast opening pneumatically actuated angle valve (VAT Group AG), hereafter referred to as the regeneration valve. The electrical valve opening time can be adjusted over a wide range. However, dead times between the electrical trigger signal and the mechanical valve motion must be considered. Therefore, the electrical trigger signal is recorded synchronously with millisecond resolution during each pulse, enabling accurate temporal alignment between regeneration valve actuation and the measured differential pressure response during regeneration. Downstream of the valve, the pulse is introduced into the clean gas side through a blow tube while the main filtration flow rate remains switched on throughout the regeneration event. The opening area of the regeneration valve is large compared to the blow tube cross-section, which has a diameter of 9 mm. The blow tube outlet is positioned such that the tube centerline is aligned with the center of the filter medium.

High speed recordings during regeneration are acquired using a Phantom Miro C321 camera. The camera provides a maximum frame rate of 1480 fps at full resolution of 1920 × 1080 pixels and is equipped with a CMOS sensor with global shutter. A ZEISS Planar T* 1.4/50 lens (focal length 50 mm, aperture range $f/1.4$ to $f/16$) is used for the recordings. To ensure sufficient and spatially uniform illumination without flicker, a LED ring light (RL12, StarLight Opto Electronics) is mounted on the inner side of the raw gas section facing the filter medium. In addition, an indicator LED is placed within the camera's field of view and lights up upon electrical regeneration valve opening, providing a visual timing reference in the recordings. The detachment process is recorded at 1000 fps, which corresponds to a temporal resolution of 1 ms per frame.

2.2. Filter medium

Two different filter media were used for the regeneration experiments: a flexible spunbond filter medium made of polyester (PES) and polyamide (PA) fibers with a hydroentangled microfilament surface (SB medium) and a rigid surface filter medium consisting of sintered polyethylene (PE) granules with a fine sintered granular polyphenylene sulfide (PPS) coating (SG medium). Fig. 3 shows scanning electron microscope (SEM) images of the SB medium (Fig. 3a) and the SG medium (Fig. 3b).

The most relevant filter medium properties are summarized in Table 1. For the regeneration experiments, the pronounced differences in thickness and the resistance of the clean filter medium (calculated with Eq. (2)) are particularly important. Since the fine coating does not fully cover the supporting coarse granular structure, the SG medium exhibits a strongly inhomogeneous surface.

For experiments with the SB medium, a new filter sample was used for each test. Prior to the experiments, the SB samples were pre-characterized with respect to initial differential pressure and clean filter medium mass. Only samples within ±10 % deviation from a reference sample were used.

In contrast, experiments with the SG medium were conducted with the same sample whenever possible, owing to the limited number of available samples and the large sample to sample structural variation. To enable reuse, the filter medium was cleaned after each test. This routine cleaning comprised brushing off residual dust and removing remaining particles by blowing compressed air through the medium. Before each experiment, the initial differential pressure was checked. If it had increased substantially, the filter medium was removed and subjected to an extended cleaning procedure, consisting of immersion in an ultrasonic bath with distilled water for 45 min. The medium was subsequently dried overnight in an oven. During ultrasonic cleaning, two SG samples were damaged. Therefore, new samples had to be used for the subsequent experiments. An overview of which experiments were performed with which SG sample is provided in Table 3 in Section 2.4.4.

2.3. Test dust

As test dust, Mikhart MU 08 (Provencale) is used in this study. The median volume based particle diameter is $x_{50,3} = 1\,\mu m$, determined offline by laser diffraction, and the relative span $\left(\frac{x_{90,3}-x_{10,3}}{x_{50,3}}\right)$ is 2.03. Mikhart MU 08 is a white, fine powder with a strong tendency to form agglomerates. Due to its high fine particle fraction, it is considered representative of materials relevant for vacuum drying. In such processes, fine particles are assumed to be preferentially entrained by the vapor flow.

2.4. Experimental procedure, parameters and data analysis

2.4.1. Experimental procedure for clean filter medium differential pressure characterization

Before conducting the filter cake detachment experiments, the clean filter media are characterized with respect to their differential pressure response during regeneration in order to identify suitable regeneration

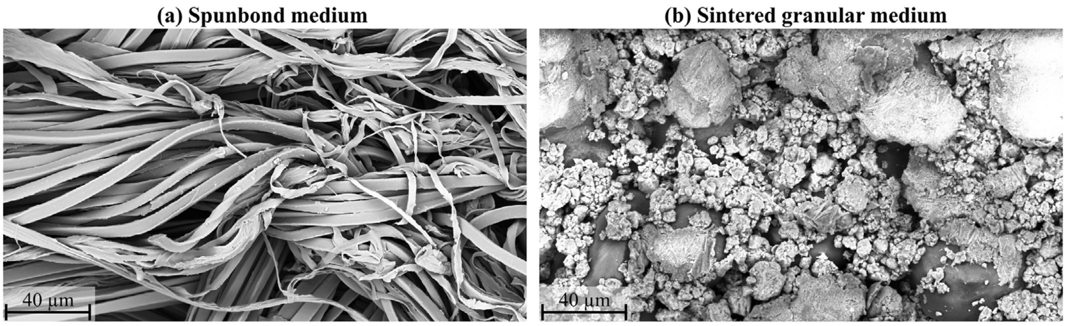

Fig. 3. SEM images of the filter media surface: (a) spunbond medium and (b) sintered granular medium with a sintered coating.

Table 1
Overview of filter medium parameters.

Name	Label	Thickness /mm	Basis weight /g m^{-2}	K1/m^{-1} at $v_F = 5.5\,\mathrm{cm\,s^{-1}}$, $p_{abs} = 100\,\mathrm{hPa}$
Spunbond medium	SB	1_a	240_a	$1.16 \cdot 10^8_b$
Sintered granular medium	SG	4_a	2148_a	$8.73 \cdot 10^8_b$

(a) From data sheet; (b) Determined with Eq. (2).

conditions for the subsequent cake detachment tests. The differential pressure during regeneration, Δp_{Reg}, is measured while varying the electrical valve opening time t_V, the tank pressure p_T, the absolute pressure p_{abs}, and the filter face velocity v_F. At $p_{\mathrm{abs}} = 900\,\mathrm{hPa}$, t_V and p_T are varied in the ranges $t_V = 100$ to $300\,\mathrm{ms}$ and $p_T = 1.5$ to $5.0 \cdot 10^5\,\mathrm{Pa}$ for $v_F = 2$ and $5.5\,\mathrm{cm\,s^{-1}}$. Subsequently, the influence of absolute pressure is assessed at $p_{\mathrm{abs}} = 900$, 100, 25, and $10\,\mathrm{hPa}$ using fixed reference settings for t_V and p_T. For SG, the p_{abs} variation is additionally repeated at two representative tank pressure levels. The specific reference settings and the resulting pulse characteristics are reported in Section 3.1.

2.4.2. Experimental procedure for regeneration experiments

The experimental procedure for the regeneration experiments comprises two consecutive steps: filter cake build-up (Fig. 4(a)) and subsequent filter cake detachment by pulse-jet regeneration (Fig. 4(b)). The Figure presents the evolution of the differential pressure Δp for a representative experiment for the SB medium and thereby illustrates both steps, which are described in more detail below. For clarity, differential pressure values reported with p_{abs} given in parentheses refer to the differential pressure at the respective operating absolute pressure, whereas values reported without p_{abs} in parentheses refer to differential pressures measured at ambient conditions. In Fig. 4, the Δp axis follows the sign convention used during cake build-up. Δp is positive and increases as the filter cake is built-up. During pulse-jet regeneration, Δp starts from a positive level and decreases, crossing into negative values. In Section 3, however, differential pressures during regeneration are plotted with inverted sign for improved readability and comparison.

2.4.3. Filter cake build-up

Before filter cake build-up is started, the mass of the clean filter medium sample is determined. After installing the filter medium in the filter chamber, the differential pressure of the unloaded medium, Δp_{FM}, is measured at ambient conditions (Fig. 4(a)). The aerosol generation system is then started and, after stabilization, connected to the filter chamber. This connection causes a short disturbance in the volumetric flow rate and, consequently, brief deviations in filter face velocity and absolute pressure, which subside once the system has stabilized.

During filter cake build-up, the total differential pressure increases approximately linearly (Fig. 4(a)). Different stopping criteria are applied for the two filter media. For the SB medium, cake build-up is stopped once a total differential pressure of about $\Delta p_{\mathrm{Tot}} = 25\,\mathrm{hPa}$ is reached, which typically requires approximately 2.5 h. This corresponds to a filter cake differential pressure of approximately $\Delta p_{\mathrm{FC}} = 24\,\mathrm{hPa}$ (see Table 2). For the SG medium, preliminary experiments showed a comparatively large scatter in the differential pressure development during cake build-up (Löschner et al., 2026a), which is also reflected in the resulting cake differential pressure (Table 2). Therefore, cake build-up for the SG medium is performed for a fixed duration of approximately 2.5 h, resulting in a mean filter cake differential pressure of 8705 Pa (Table 2). As shown in Table 2, this approach yields comparable cake mass loadings per unit area, for both filter media. After reaching the stopping criterion, the aerosol supply is disconnected, which again induces short flow fluctuations. The system is then allowed to stabilize before the final total differential pressure is recorded. The differential pressure contribution of the filter cake is obtained from Eq. (1) as $\Delta p_{\mathrm{FC}} = \Delta p_{Tot} - \Delta p_{\mathrm{FM}}$.

Table 2
Overview of filter cake build up results.

Filter medium	Mean filter cake differential pressure /Pa	Mean mass loading /g m^{-2}
Spunbond medium	2417 ± 106	49.4 ± 5.1
Sintered granular medium	8705 ± 1754	47.9 ± 6.2

All cake build up experiments are performed at an absolute pressure of 900 hPa and a filter face velocity of $v_F = 5.5\,\mathrm{cm\,s^{-1}}$. This choice is motivated by previous results indicating that the resulting cake structure is approximately independent of absolute pressure, while the effort for cake preparation is substantially reduced and comparability is improved because all cakes are generated under identical conditions (Löschner et al., 2026a). After cake build up, the filter sample is removed and weighed to determine the cake mass m_{FC} and thus the mean cake mass loading W.

2.4.4. Filter medium regeneration

For regeneration, the dust loaded filter sample is re-installed in the filter chamber. The impact of the regeneration procedure on the differential pressure evolution is illustrated in Fig. 4(b). The desired operating conditions (absolute pressure and filter face velocity) are set and, after reaching steady state, the total differential pressure at

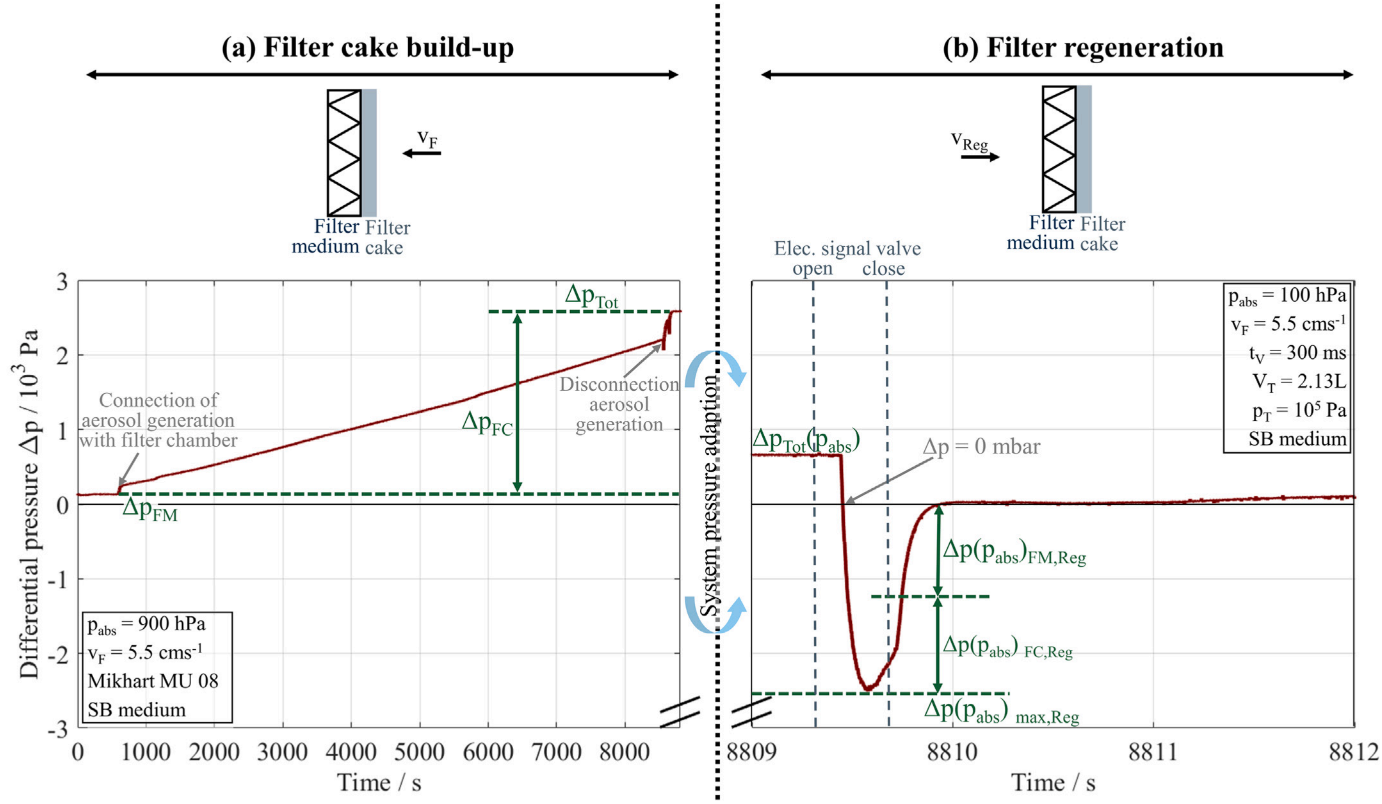

Fig. 4. Differential pressure behavior during an exemplary experiment including filter cake build up (a) and filter medium regeneration with pulse jet cleaning (b).

operating conditions $\Delta p_{\mathrm{Tot}}(p_{\mathrm{abs}})$ is recorded. Subsequently, a regeneration pulse is triggered. During the pulse, the differential pressure, the raw gas absolute pressure, and the electrical trigger signal of the regeneration valve are recorded with millisecond resolution over an acquisition window of 9 s. For all experiments, a constant electrical valve opening time of 300 ms is used. Details on the choice of t_V are provided in Section 3.1. Simultaneously, the high speed camera is triggered to record the filter cake detachment process optically. Temporal alignment between the image sequence and the pressure signals is provided by the indicator LED described in Section 2.1.3. After regeneration and re-establishing stationary flow conditions, the residual differential pressure at operating conditions $\Delta p_{\mathrm{res}}(p_{\mathrm{abs}})$ is recorded. The residual cake differential pressure is obtained as $\Delta p_{\mathrm{FC,res}}(p_{\mathrm{abs}}) = \Delta p_{\mathrm{res}}(p_{\mathrm{abs}}) - \Delta p_{\mathrm{FM}}(p_{\mathrm{abs}})$.

An overview of all investigated operating points for the filter cake detachment experiments is given in Table 3. Regeneration is investigated at two filter face velocities, $v_F = 5.5\,\mathrm{cm\,s^{-1}}$ and $v_F = 2.0\,\mathrm{cm\,s^{-1}}$. At $v_F = 5.5\,\mathrm{cm\,s^{-1}}$, four absolute pressures are studied, namely 900, 100, 25, and 10 hPa. To limit the total number of experiments, only two absolute pressures are investigated at $v_F = 2.0\,\mathrm{cm\,s^{-1}}$, namely 900 and 25 hPa. Each operating point is repeated three times. For the SB medium, a new filter sample is used for each repetition, denoted SBx. For the SG medium, the same sample is used for the three repetitions provided it remains undamaged during cleaning. The corresponding sample identifiers are listed in Table 3.

To improve comparability across different absolute pressures, the tank pressure p_T is adjusted at each operating point to reach a predefined target maximum differential pressure of the clean medium, based on the characterization results in Section 3.1. For the SG medium, two tank-pressure levels are investigated to realize two different $\Delta p_{\mathrm{Reg,max}}$ levels. These levels correspond to the reference tank pressures at $p_{\mathrm{abs}} = 900\,\mathrm{hPa}$ of $p_{T,\mathrm{high}} = 5 \cdot 10^5\,\mathrm{Pa}$ and $p_{T,\mathrm{low}} = 3 \cdot 10^5\,\mathrm{Pa}$. For the SB medium, only one $\Delta p_{\mathrm{Reg,max}}$ level can be realized due to the lower limit of achievable p_T.

2.4.5. Data processing and analysis of pressure signals during regeneration

For the data analysis, the maximum differential pressure during regeneration, $\Delta p_{\mathrm{max,reg}}$, is used as a key characteristic parameter. Note that $\Delta p_{\mathrm{max,reg}}$ is always determined at respective the operating pressure. In this work, $\Delta p_{\mathrm{max,reg}}$ is used rather than a maximum clean gas absolute pressure p_{max}, because both raw gas side and clean gas side absolute pressures can change rapidly during the pulse due to the limited volume of the raw gas section and the raw gas side pressure can therefore not be assumed constant.

In addition, $\Delta p_{\mathrm{max,reg}}$ can be split into contributions associated with flow through the filter medium and the filter cake *during the regeneration pulse* (Koch et al., 1996). This splitting is indicated schematically in Fig. 4(b).

$$\Delta p_{\mathrm{max,reg}} = \Delta p(p_{abs})_{\mathrm{FM,reg}} + \Delta p(p_{abs})_{\mathrm{FC,reg}}. \tag{7}$$

Here, $\Delta p(p_{abs})_{\mathrm{FM,reg}}$ denotes the portion of the pulse differential pressure that is required to drive the transient reverse flow through the filter medium. The remaining contribution, $\Delta p(p_{\mathrm{abs}})_{\mathrm{FC,reg}}$, acts across the filter cake layer and can therefore be interpreted as the maximum available driving load for filter cake detachment at $\Delta p_{\mathrm{max,reg}}$, as long as the filter cake is still present on the filter medium. Since filter cake detachment may already start before the differential pressure pulse maximum value is reached, the partitioning in Eq. (7) should be interpreted as an estimate of the maximum differential pressure acting on the filter cake.

The partitioning is based on the linear resistance relations introduced above (Eqs. (2) and (3)) using the resistance coefficients K_1 and K_2 determined from the steady state conditions before regeneration. From Eqs. (2) and (3), the coefficients are obtained as

$$K_1 = \frac{\Delta p_{\mathrm{FM}}}{\mu v_F}, \qquad K_2 = \frac{\Delta p_{\mathrm{FC}}}{\mu v_F W}, \tag{8}$$

with gas viscosity μ, filter face velocity v_F, and cake mass loading per unit area. Importantly, Δp_{FM} and Δp_{FC} in Eq. (8) are evaluated at the respective operating absolute pressure prior to regeneration.

Table 3
Overview of the regeneration experiments, including operating conditions and the corresponding filter medium labels used for each experiment.

Filter face velocity/cm s^{-1}	Filter medium	Absolute pressure/hPa	Tank pressure/10^5 Pa	Label filter medium
5.5	SB	900	5.00	SB1-SB3
		100	1.41	SB4-SB6
		25	1.00	SB7-SB9
		10	1.00	SB10-SB12
	SG (high)	900	5.00	A
		100	1.98	A
		25	1.60	A
		10	1.44	B, C, C
	SG (low)	900	3.00	A
		100	1.10	A
		25	1.00	A
		10	1.00	B
2.0	SB	900	5.00	SB13-SB15
		25	1.00	SB16-SB18
	SG (high)	900	5.00	C
		25	1.75	C
	SG (low)	900	3.00	C
		25	1.10	C

The unloaded medium differential pressure Δp_{FM} is measured directly at 900 hPa for each filter sample. For reduced absolute pressures, $\Delta p(p_{abs})_{\mathrm{FM}}$, and thus K_1, is estimated using a scaling approach based on a reference sample $S1$ for which $\Delta p(p_{abs})_{\mathrm{FM}}$ was measured as a function of p_{abs} Löschner et al. (2026b). For a different sample $S2$ of the same media, the unloaded medium differential pressure at operating absolute pressure is then approximated by

$$\Delta p_{\mathrm{FM},S2}(p_{\mathrm{abs}}) = \Delta p_{\mathrm{FM},S1}(p_{\mathrm{abs}}) \cdot \frac{\Delta p_{\mathrm{FM},S2}(900\,\mathrm{hPa})}{\Delta p_{\mathrm{FM},S1}(900\,\mathrm{hPa})} \tag{9}$$

and finally, K_1 for the respective sample can be calculated using Eq. (8). The total differential pressure at operating absolute pressure is recorded before regeneration. Consequently, the filter cake differential pressure at operating conditions is obtained from Eq. (1) as $\Delta p(p_{abs})_{\mathrm{FC}} = \Delta p(p_{abs})_{\mathrm{Tot}} - \Delta p(p_{abs})_{\mathrm{FM}}$ and K_2 can be calculated Eq. (8).

Using these coefficients, the pulse peak can be partitioned as

$$\Delta p(p_{abs})_{\mathrm{FM,reg}} = \frac{K_1}{K_1 + K_2 W}\,\Delta p_{\mathrm{max,reg}}, \tag{10}$$

and

$$\Delta p(p_{abs})_{\mathrm{FC,reg}} = \frac{K_2 W}{K_1 + K_2 W}\,\Delta p_{\mathrm{max,reg}}. \tag{11}$$

Another characteristic quantity for evaluating the regeneration pulse is the differential pressure rise rate, i.e., the first time derivative of the differential pressure. According to the literature, this parameter is also relevant for filter cake detachment. To determine the maximum differential pressure rise rate, $\left(\mathrm{d}\Delta p_{\mathrm{Reg}}/\mathrm{d}t\right)_{\mathrm{max}}$, the measured signal $\Delta p_{\mathrm{Reg}}(t)$ is smoothed by time binning and differentiated using first differences. The time coordinate of the maximum is denoted $t_{\mathrm{RR,max}}$ (with RR referring to rise rate). The procedure is described in Appendix B.

2.4.6. Image analysis for the determination of the optical cleaning efficiency E_{opt}

The determination of the optical cleaning efficiency E_{opt} from the high speed image acquisitions is described in the following. The workflow is illustrated in Fig. 5. The individual processing steps are shown for the SG medium as an example.

At the beginning, a frame recorded approximately 1 s before the electric opening signal of the regeneration valve is selected (Fig. 5 (1)). This frame represents the undisturbed filter cake prior to the pulse. A circular region of the filter cake is then selected on the image to define the filter surface. The circle diameter corresponds to the known filter diameter of 14 cm. The selected frame is converted to grayscale and stored as the reference image (Fig. 5 (2)). Next, a frame recorded approximately 8 ms after the start of the pulse is selected (Fig. 5 (3)). This frame is chosen to allow detached dust to settle and thereby minimize interference with the evaluation. The selected frame is also converted to grayscale and stored.

Subsequently, a pixel wise difference image is computed between the reference image and the last frame (Fig. 5 (4)). The resulting difference image contains gray scale differences in the range from 0 to 255. To clearly separate areas where the cake was removed from areas with remaining filter cake, the difference image is converted into a binary image (Fig. 5 (5)). This requires a threshold value that classifies pixels as either ‘filter cake removed’ (white) or ’filter cake remaining’ (black). The threshold is determined automatically using Otsu’s method (Otsu, 1979), which selects the value that best separates the two classes based on the grayscale histogram. The automatically determined threshold was visually verified for each recording and adjusted manually in the few cases where it did not separate cleaned and cake covered regions correctly. Finally, pixels classified as ’filter cake removed’ in the binary image are highlighted in red on the original last frame (Fig. 5 (6)) to visualize the regenerated area. The red pixel area is summed to obtain the regenerated filter area, which is used to calculate E_{opt} according to Eq. (4).

3. Results and discussion

3.1. Characterization of the differential pressure behavior during regeneration of clean filter media

Characterization experiments are performed with clean filter media to separate the pulse generation and propagation in the setup from effects related to filter cake cracking, lift off, and particle detachment. In this way, the influence of operating conditions on the pulse shape and key pulse metrics (such as $\Delta p_{Reg,\mathrm{max}}$) can be assessed without additional variability introduced by the dust layer. All regeneration experiments in this section are performed with particle free air.

For the characterization part, only experiments at a filter face velocity of $v_F = 5.5\,\mathrm{cm\,s^{-1}}$ are presented. A reduction of the filter face velocity did not lead to qualitative changes in the transient differential pressure behavior.

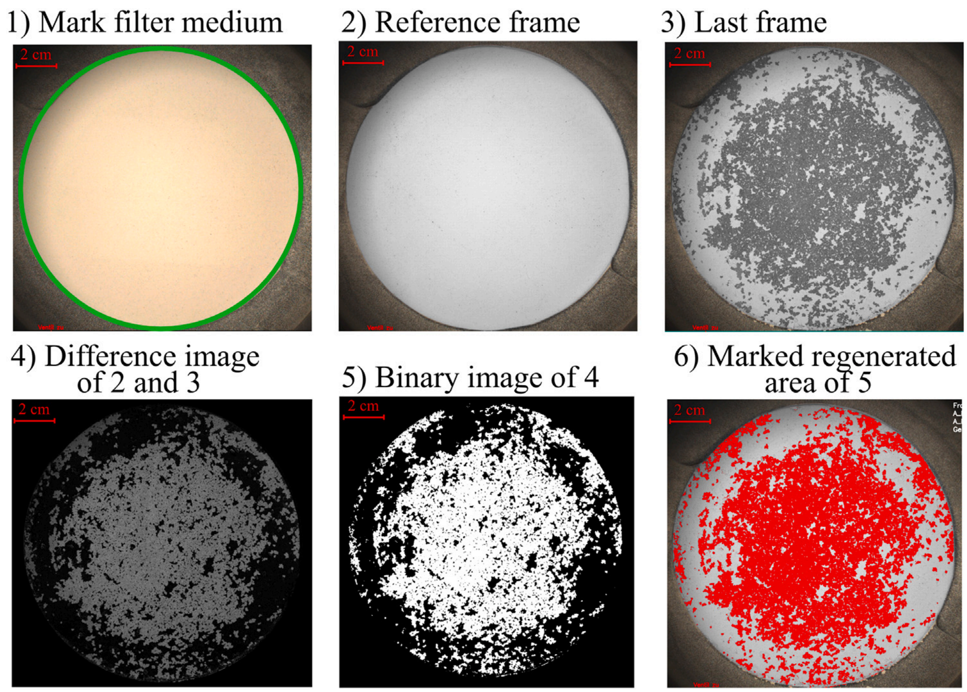

Fig. 5. Workflow for the determination of the optical cleaning efficiency E_{opt} from high speed images.

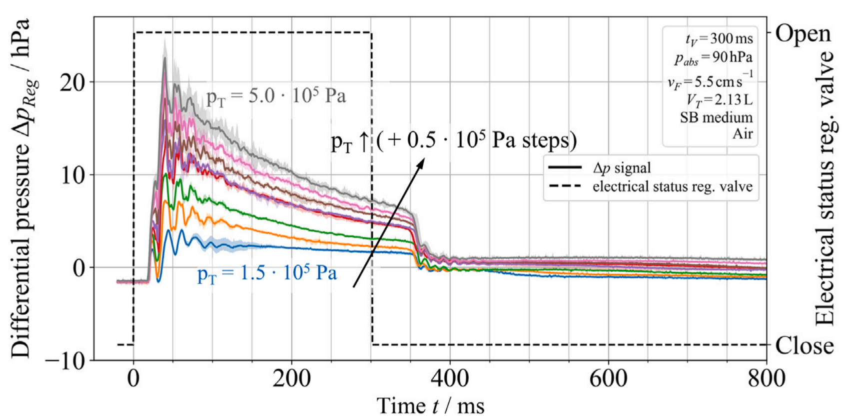

Fig. 6. Differential pressure $\Delta p(t)$ during regeneration for varying tank pressure p_T at $p_{abs} = 900$ hPa, $t_V = 300$ ms, and $v_F = 5.5$ cm s^{-1} (SB medium). p_T is increased from $1.5 \cdot 10^5$ Pa to $5.0 \cdot 10^5$ Pa in $0.5 \cdot 10^5$ Pa steps. Solid lines show $\Delta p(t)$; dashed lines indicate the electrical valve signal.

The valve opening time is investigated first. This variation shows that a value of $t_V = 300$ ms ensures a fully developed pulse for both filter media. Therefore, $t_V = 300$ ms is used for all following experiments. The corresponding results are presented and discussed in Appendix A.

3.1.1. Influence of tank pressure

In this section, the influence of tank pressure on the differential pressure response during regeneration is investigated. Fig. 6 shows the tank pressure variation for the SB medium. Operating conditions and presentation are given in the caption.

An increase in tank pressure primarily shifts the maximum differential pressure $\Delta p_{max,Reg}$ to higher values, while the onset of the pulse and the overall timing of the differential pressure rise remain essentially unchanged. In the present data, $\Delta p_{max,Reg}$ increases approximately linearly from 402 Pa at $p_T = 1.5$ bar to 2256 Pa at $p_T = 5$ bar, whereas the onset delay remains about 20 ms after electric valve actuation. This trend is consistent with literature findings reporting that tank pressure mainly controls pulse strength metrics such as $\Delta p_{max,Reg}$ and $d\Delta p/dt$, whereas the characteristic timing of the initial pressure rise is comparatively insensitive (Leubner and Riebel, 2004). The SG medium behaves analogously and is therefore not shown.

3.1.2. Influence of absolute pressure

In a next step, the differential pressure response during regeneration was investigated at different absolute pressures while keeping the tank pressure constant (SB medium, Fig. 7; operating conditions see caption).

Decreasing the absolute pressure leads to two systematic changes in the transient differential pressure behavior. The maximum differential pressure $\Delta p_{max,Reg}$ increases, and the pressurization phase extends over a longer time so that the maximum is reached later. The later maximum does not indicate a delayed onset of the pulse. At a given time early in the pulse, the differential pressure at reduced absolute pressure already exceeds the maximum reached at 900 hPa. The pulse therefore rises to a higher peak and the pressure build up lasts longer. The time of the maximum $t_{\Delta p_{max,Reg}}$ increases from about 44 ms at 900 hPa to 123 ms at 100 hPa, 163 ms at 25 hPa, and 177 ms at 10 hPa. A further notable observation is that the pronounced oscillations visible at $p_{abs} = 900$ hPa

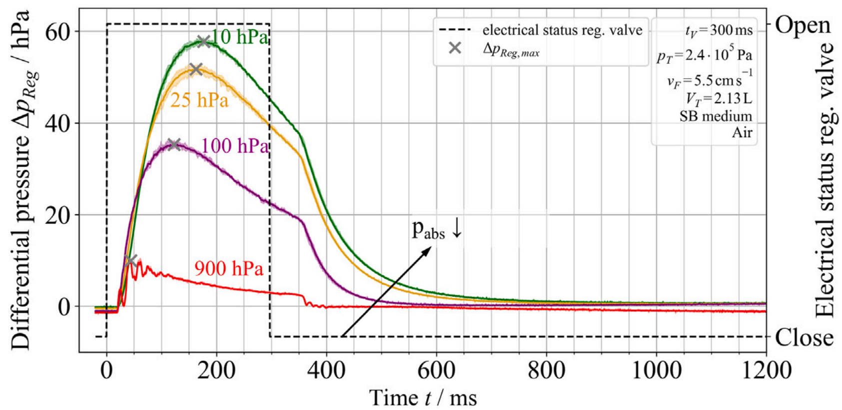

Fig. 7. Differential pressure $\Delta p(t)$ during regeneration for varying absolute pressure p_{abs} at constant tank pressure $p_T = 2.4 \cdot 10^5$ Pa, $t_V = 300$ ms, and $v_F = 5.5$ cm s^{-1} in air (SB medium). Absolute pressure is reduced from 900 hPa to 10 hPa. Solid lines show $\Delta p(t)$; dashed lines indicate the electrical valve signal.

are no longer apparent at reduced absolute pressure. The corresponding measurements for the SG medium show the same qualitative trends and are therefore not shown.

Two mechanisms explain these changes. First, the higher peak results from the strongly increasing pressure ratio p_T/p_{abs} at constant p_T. For the conditions studied here, p_T/p_{abs} increases from approximately 2.7 at 900 hPa to 24 at 100 hPa, 96 at 25 hPa, and 240 at 10 hPa. This increasing ratio intensifies the pulse injection and thus the transient pressurization of the clean gas side and the raw gas side. In addition, at lower p_{abs} the gas mass initially contained in the relevant volumes (clean and raw gas side) is substantially smaller. If a comparable amount of gas is injected during the pulse event, the resulting pressure rise becomes larger in relative terms, which directly contributes to an increased $\Delta p_{Reg,\max}$. Second, the later occurrence of the maximum is consistent with a longer effective pressurization phase under highly expanded conditions. At reduced p_{abs}, the transient development of the absolute pressures on both sides of the filter element becomes more pronounced. In particular, the raw gas side absolute pressure responds noticeably during the pulse (cf. Section 2.4.5). As a consequence, $\Delta p(t)$ reflects the coupled dynamics of clean gas pressurization and the simultaneous response of the raw gas side, which can delay the time at which the maximum differential pressure is reached.

3.1.3. Parameter selection for the filter cake detachment experiments

Since $\Delta p_{Reg,\max}$ is commonly considered a key parameter governing regeneration performance (Leubner and Riebel, 2004), a constant tank pressure across all p_{abs} would result in substantially different pulse strengths. The tank pressure was therefore adjusted for each absolute pressure such that a common target maximum differential pressure $\Delta p_{\max,target}$ was reached as closely as possible (Section 2.4.4). The target values were defined as the maximum values measured at $p_{abs} = 900$ hPa under selected reference conditions: a single setting for SB (high level) and two settings for SG (high level and low level).

The resulting differential pressures are shown in Fig. 8 for the SB medium (a) and the SG medium (b). The corresponding tank pressures for each operating point are summarized in Table 3.

For the SB medium (Fig. 8a), $\Delta p_{Reg,\max}$ can be kept approximately constant for $p_{abs} = 900$, 100, and 25 hPa by reducing p_T accordingly. At $p_{abs} = 10$ hPa, however, the required tank pressure to match the target $\Delta p_{Reg,\max}$ would be below ambient pressure, which is not feasible in the present experimental setup. Consequently, $\Delta p_{Reg,\max}$ at 10 hPa remains higher than the target level, which must be considered when comparing regeneration results (e.g., cleaning efficiencies) across different absolute pressures. In addition, Fig. 8(a) shows that the maximum differential pressure value is reached earliest at 900 hPa and shifts to later times as p_{abs} is reduced. This behavior is consistent with slower transient pressurization at reduced operating pressure when the tank pressure is lowered to meet the same $\Delta p_{\max,target}$, i.e., a smaller driving pressure and reduced gas density lead to a lower transient mass flux into the clean gas side and thus to a slower rise of $\Delta p(t)$. Correspondingly, the initial differential pressure rise becomes less steep as p_{abs} decreases.

For the SG medium (Fig. 8b), the same qualitative trends are observed. In contrast to the SB medium, $\Delta p_{Reg,\max}$ can be matched closely for all investigated p_{abs} by adjusting p_T. A further distinct feature for SG is that $\Delta p_{Reg,\max}$ at reduced absolute pressure is reached at the time of mechanical valve closing. This indicates that the build-up of $\Delta p(t)$ is still ongoing up to the end of the valve opening interval. Consequently, increasing t_V would likely increase $\Delta p_{Reg,\max}$ for SG at otherwise identical conditions, although this was not investigated here.

Fig. 9 summarizes the achieved maximum differential pressures $\Delta p_{Reg,\max}$ as a function of absolute pressure for $v_F = 5.5$ cm s^{-1} (a) and $v_F = 2.0$ cm s^{-1} (b). The annotated values next to the symbols report the tank pressures p_T required to meet the target values at the respective operating points. The behavior of the SB medium and of the SG medium at the high level at $v_F = 5.5$ cm s^{-1} follows the trends already described with Fig. 8. The following description therefore focuses on the SG medium at the low level and on the comparison of the two filter face velocities.

At $v_F = 5.5$ cm s^{-1} (Fig. 9a), the SG low level follows the target $\Delta p_{Reg,\max}$ well over most of the pressure range. The clearest deviation occurs at $p_{abs} = 10$ hPa. There the SG low level exceeds the target for the same reason as the SB medium, since the tank pressure p_T is already at the lower limit of the setup and cannot be reduced further.

The comparison with the lower filter face velocity $v_F = 2.0$ cm s^{-1} (Fig. 9b) shows the same overall picture. The target $\Delta p_{Reg,\max}$ is met closely for the SB medium and for the SG medium at the high level. For the SG medium at the low level a small deviation remains at $p_{abs} = 25$ hPa. This results from the limited range of adjustable tank pressures.

3.2. Regeneration behavior of surface filter media at reduced absolute pressure with pulse-jet cleaning

This Section addresses filter cake detachment and the influence of reduced absolute pressure on the detachment dynamics.

3.2.1. High speed image sequences

Selected frame sequences from the high speed recordings are used to visualize the filter cake detachment process and to relate the observed detachment dynamics to the simultaneously measured differential pressure $\Delta p(t)$. The sequences shown here are exemplary and are restricted to four operating points, namely $p_{abs} = 900$ hPa and 25 hPa for the spunbond medium (SB) (Figs. 10 and 11) and for the sintered granular medium (SG) (Figs. 12 and 13). The influence of the operating

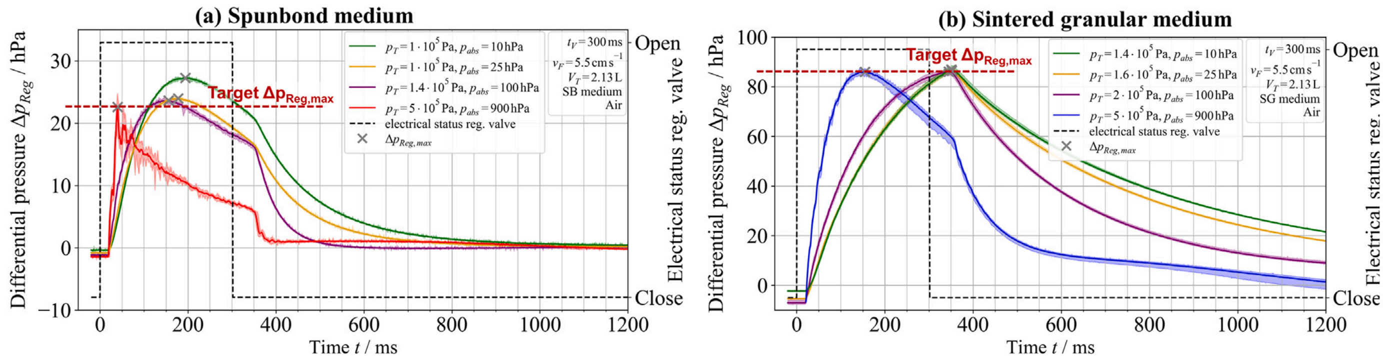

Fig. 8. Differential pressure $\Delta p(t)$ during regeneration for varying absolute pressure p_{abs} with adjusted tank pressure p_T to reach a target maximum differential pressure $\Delta p_{max,target}$ at $t_V = 300\,ms$ and $v_F = 5.5\,cm\,s^{-1}$ (a) SB medium and (b) SG medium. Solid lines show $\Delta p(t)$; dashed lines indicate the electrical valve signal.

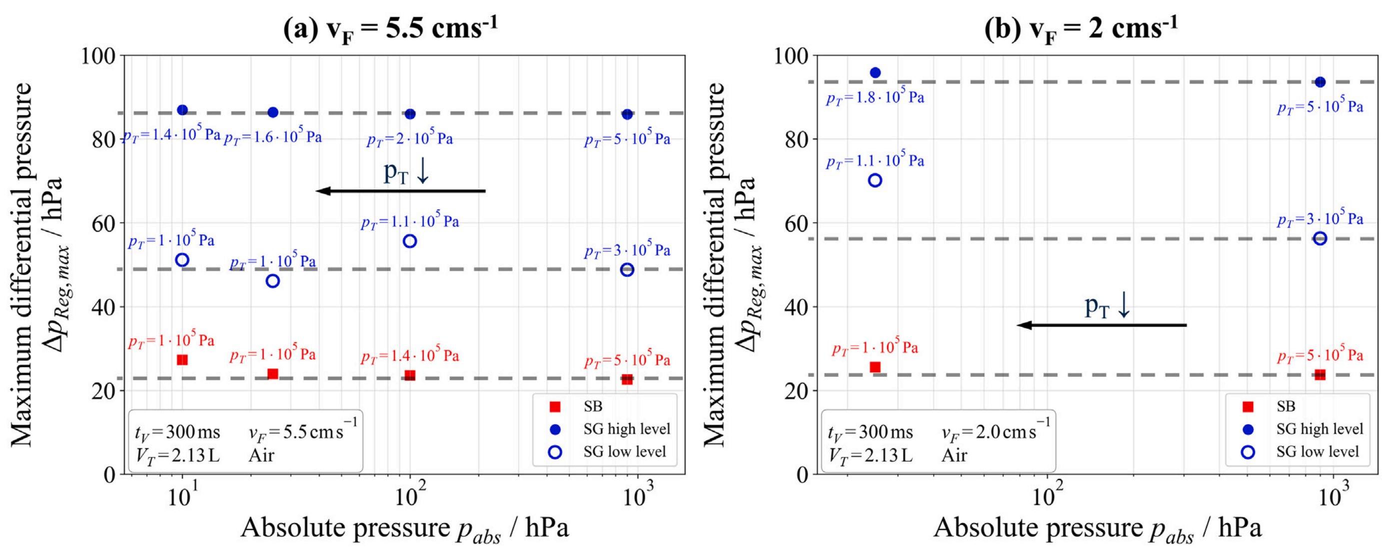

Fig. 9. Maximum differential pressure $\Delta p_{Reg,max}$ as a function of absolute pressure p_{abs} with tank pressure adjusted to reach $\Delta p_{max,target}$ at $t_V = 300\,ms$ (a) $v_F = 5.5\,cm\,s^{-1}$ and (b) $v_F = 2.0\,cm\,s^{-1}$. SB red symbols. SG blue symbols: filled symbols high level, open symbols low level. Dashed lines indicate the corresponding target levels at $p_{abs} = 900\,hPa$.

parameters (v_F and p_T) is discussed in the following sections based on quantitative measures, in particular the onset of detachment (first detectable cake release) and the resulting cleaning efficiencies.

For each sequence nine individual frames are shown in Figs. 10–13: the frame at start of the electrical regeneration valve opening time, the frame at $\Delta p = 0\,Pa$, the frame at first detected local detachment, three to four frames within 9 to 74 ms after first detachment, the frame at the maximum differential pressure $\Delta p_{Reg,max}$, the frame at the end of the electrical valve signal ($t = 300\,ms$), and the last recorded frame ($t = 8000\,ms$). The corresponding videos are provided in the supplementary material. For the frame of first filter cake detachment, the areas where cake is released are marked by red boundary lines.

SB medium. For the SB medium at $p_{abs} = 900\,hPa$ (Fig. 10), the onset of detachment occurs essentially when the differential pressure reaches $\Delta p = 0\,Pa$, i.e., when the driving pressure difference changes sign and the flow through the medium reverses. Immediately after this point, the cake is removed very rapidly and in a highly dispersed manner: detached material forms a fine dust cloud near the filter surface and the detachment process is largely completed within a few tens of milliseconds. When $\Delta p_{Reg,max}$ is reached, the filter cake has already been removed and subsequent frames predominantly show settling of airborne dust rather than additional detachment. This is consistent with the similarity of the frames at $t = 300\,ms$ (end of electrical valve signal) and $t = 8000\,ms$, indicating that the relevant detachment event is completed long before the valve signal ends.

At $p_{abs} = 25\,hPa$ (Fig. 11) for the SB medium, the first detachment is again detected close to $\Delta p = 0\,Pa$, confirming that the onset is tied to the beginning of flow reversal. Compared to 900 hPa, the detachment proceeds slightly more slowly and the spatial detachment pattern becomes more structured. In the shown example, cake removal initiates preferentially in regions influenced by the support structure and near the rim and progresses across the filter surface over several tens of milliseconds. This detachment pattern (preferential release along the support structure and at the rim) is consistently observed for the SB medium at reduced absolute pressures for both investigated filter face velocities, and it becomes more pronounced as p_{abs} is decreased further. Nevertheless, for SB the main removal still takes place early in the pulse. Importantly, $\Delta p(t)$ continues to rise after the visually dominant detachment phase is largely completed, and $\Delta p_{Reg,max}$ occurs substantially later. Previous work on pulse jet cleaning likewise emphasizes that regeneration cannot be interpreted solely based on $\Delta p_{Reg,max}$, but depends strongly on the early time development of the pulse and the pulse dynamics (Leubner and Riebel, 2004). In Section 3.2.2, this aspect is examined quantitatively by relating the onset of detachment both to the maximum differential pressure during regeneration $\Delta p_{Reg,max}$ and to the maximum differential pressure rise rate $\left(d\Delta p_{Reg}/dt\right)_{max}$, which is expected to be more representative for the initial detachment than $\Delta p_{Reg,max}$.

SG medium. The detachment behavior of the SG medium differs fundamentally from that of the SB medium. At $p_{abs} = 900\,hPa$ (Fig. 12),

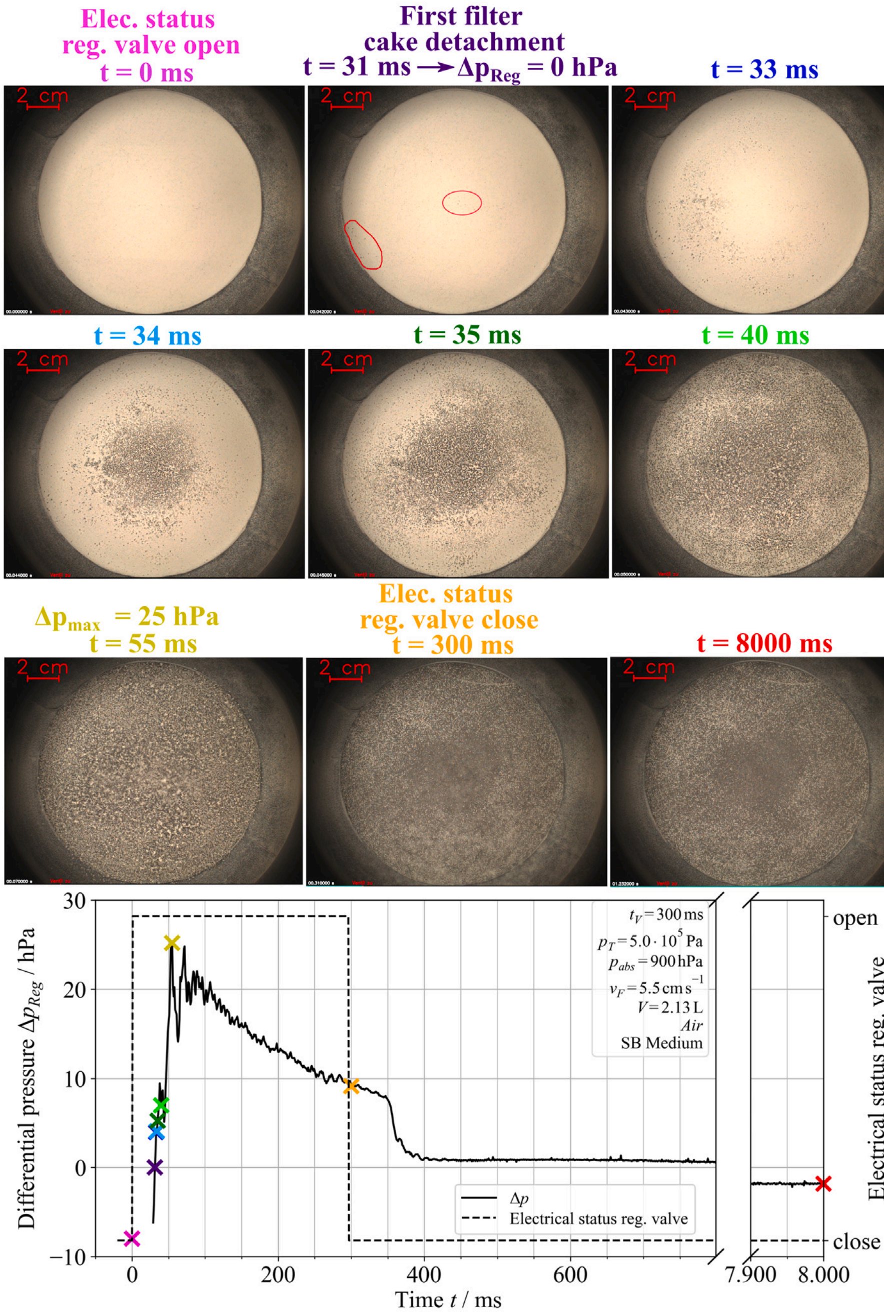

Fig. 10. Selected frame sequence and differential pressure $\Delta p(t)$ for SB filter cake detachment at $p_{\text{abs}} = 900\,\text{hPa}$, $t_V = 300\,\text{ms}$, and $v_F = 5.5\,\text{cm}\,\text{s}^{-1}$. The selected frame time stamps are color coded and the corresponding time points are marked on $\Delta p(t)$ using the same colors.

$\Delta p = 0\,\text{Pa}$ is reached at approximately $t = 70\,\text{ms}$, but the first visible filter cake detachment occurs later, at $t \approx 92\,\text{ms}$, when the differential pressure has already increased to $\Delta p \approx 2.5 \cdot 10^3\,\text{Pa}$. Hence, for the rigid SG medium the onset of detachment requires a distinctly higher differential pressure level than merely the sign change at $\Delta p = 0\,\text{Pa}$. After onset, detachment proceeds in a more coherent and fragment like manner. Rather than an immediately fine dispersion, larger fragments and extended cake areas are released and the cleaned area develops progressively. In this case, the cake is already detached around the time $\Delta p_{Reg,\max}$ is reached. However, the corresponding frame can still show pronounced settling cake fragments, as part of the detached material remains airborne and has not yet fully sedimented. Consistent with the higher flow resistance and the rigidity of the SG medium (see Introduction), a larger fraction of the pulse is consumed by the differential pressure across the medium before sufficiently high flow forces act on the cake to initiate detachment.

At $p_{\text{abs}} = 25\,\text{hPa}$ (Fig. 13) for the SG medium, the detachment dynamics change again. While $\Delta p = 0\,\text{Pa}$ is reached early (around $t = 41\,\text{ms}$, i.e., about 30 ms earlier than for SG at 900 hPa), the first visible detachment is detected only at $t \approx 106\,\text{ms}$, i.e., later than at 900 hPa even though flow reversal occurs earlier. This apparent contradiction is explained by the slower increase of $\Delta p(t)$ at reduced absolute pressure, as discussed in the pulse characterization section. A slower pressure build up on the clean gas side delays the attainment of the differential pressure level required for detachment. In addition, detachment is visibly more localized at 25 hPa. It starts from a comparatively small region and then spreads outward across the filter surface, forming a growing dust cloud and expanding cleaned area over a markedly longer

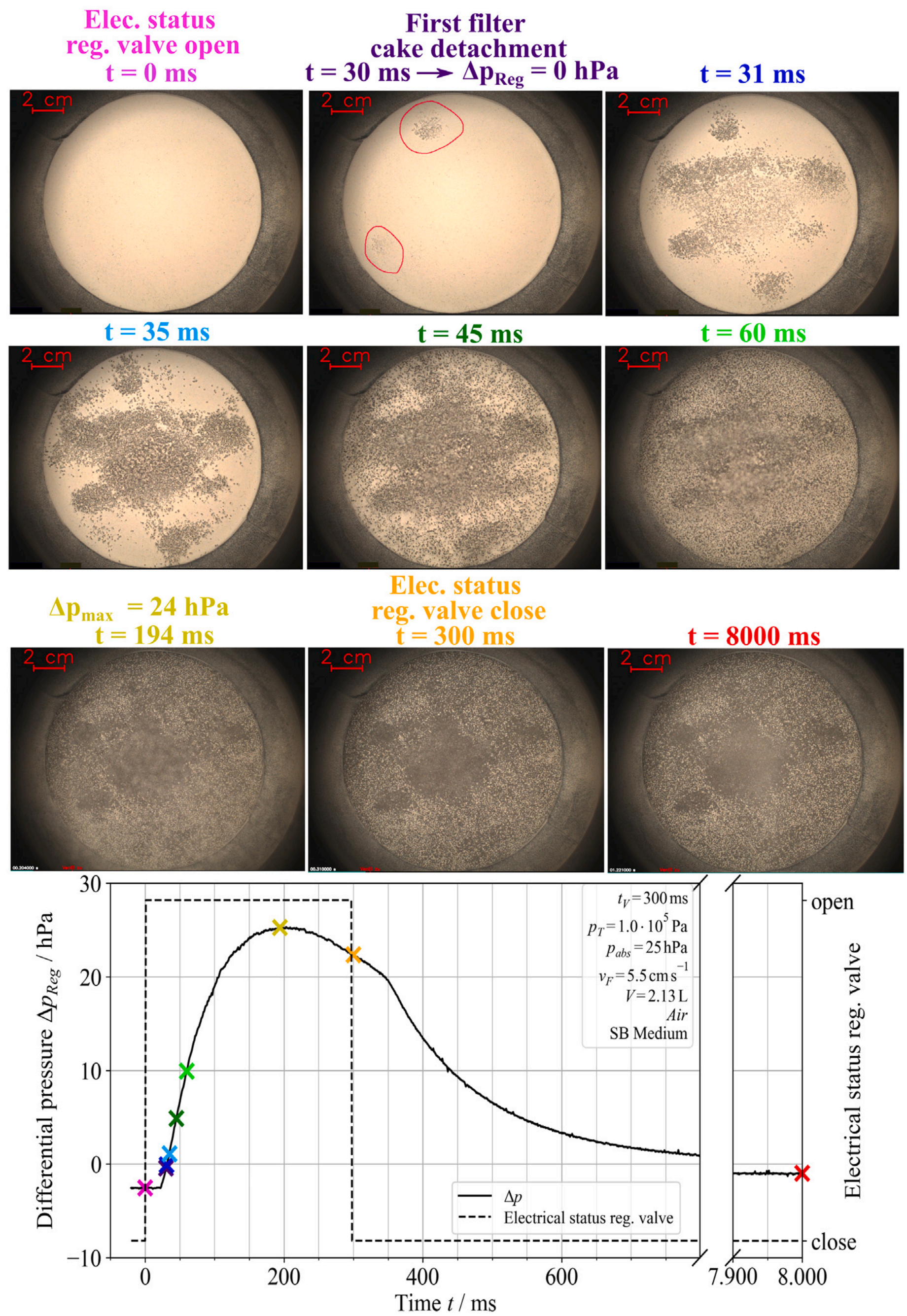

Fig. 11. Selected frame sequence and differential pressure $\Delta p(t)$ for SB filter cake detachment at $p_{abs} = 25\,\text{hPa}$, $t_V = 300\,\text{ms}$, and $v_F = 5.5\,\text{cm}\,\text{s}^{-1}$. Presentation as in Fig. 10.

time interval than observed at ambient pressure. In contrast to SB (and also in contrast to SG at 900 hPa), substantial changes are still visible up to the time when $\Delta p_{Reg,\max}$ occurs. $\Delta p_{\max,Reg}$ even exceeds the mechanical valve closing, indicating that the differential pressure continues to increase throughout the valve opening interval and that cake removal can extend up to the maximum differential pressure at reduced absolute pressure. The final frames show that a peripheral residual ring and local deposits remain, i.e., detachment is incomplete for this operating point despite the prolonged detachment phase.

3.2.2. Influences of pulse strength on the onset of filter cake detachment

Motivated by the observations in Section 3.2.1, the onset of filter cake detachment is quantified as a function of the filter medium structure, the absolute pressure p_{abs}, the pulse strength set via the tank pressure p_T, and the filter face velocity v_F. The onset time t_{det} is defined as the time from the electrical valve opening signal at $t = 0$ to the first clearly visible change of the filter cake between two consecutive high-speed frames. The onset time is first estimated with a Python routine and then confirmed manually by identifying the frame with the first visible change of the filter cake between two consecutive frames. At the recording rate of 1000 fps the resulting uncertainty of t_{det} is on the order of 1 ms.

Influence of absolute pressure on t_{det}. Fig. 14 summarizes t_{det} as a function of p_{abs} for both media and both filter face velocities; the symbols are explained in the caption. The arrow indicates that p_T was reduced with decreasing p_{abs} to keep $\Delta p_{Reg,\max}$ of the clean medium close to the target value (Section 3.1).

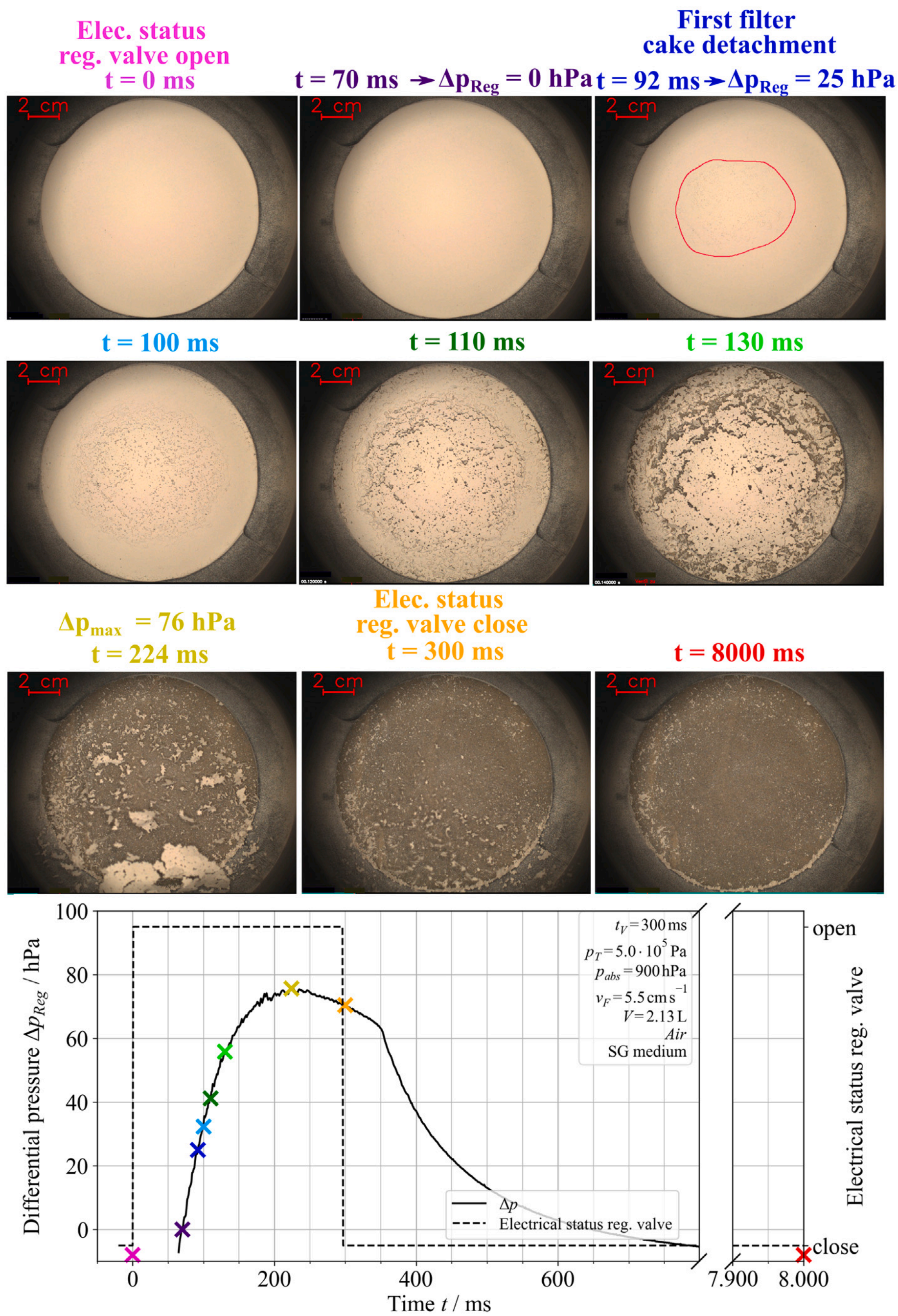

Fig. 12. Selected frame sequence and differential pressure $\Delta p(t)$ for SG filter cake detachment at p_{abs} = 900 hPa, pulse strength high level, t_V = 300 ms, and $v_F = 5.5\,\mathrm{cm\,s^{-1}}$. Presentation as in Fig. 10.

For the SB medium, t_{det} shows no pronounced dependence on p_{abs} over the investigated range. Detachment starts consistently very early (on the order of a few 10 ms), which matches the qualitative observation from the exemplary frame sequences: the first visible detachment occurs essentially when $\Delta p(t)$ reaches 0 Pa and the flow reverses. A systematic influence of v_F is, however, visible. At $v_F = 2.0\,\mathrm{cm\,s^{-1}}$ the onset tends to occur earlier than at $v_F = 5.5\,\mathrm{cm\,s^{-1}}$. This is consistent with the fact that the differential pressure before regeneration scales with v_F (Eqs. (2)–(3)). Hence, at lower v_F a smaller opposing differential pressure has to be compensated until $\Delta p(t)$ reaches zero and the flow reverses. In addition, lower filtration velocities are commonly associated with less compacted cakes and reduced adhesion, which can facilitate earlier detachment (Silva et al., 1999).

In contrast, the SG medium exhibits substantially delayed onset times and a clear dependence on both pulse strength level and p_{abs}. At a given p_{abs}, the higher pulse strength level leads to earlier detachment than the lower pulse strength level. Moreover, decreasing p_{abs} tends to shift t_{det} to later times, particularly for the low tank pressure level. This trend is consistent with the characterization results: at reduced p_{abs}, the increase of $\Delta p(t)$ is less steep and the maximum value is reached later when p_T is lowered to keep $\Delta p_{Reg,max}$ comparable. Since detachment on the rigid SG medium does not start at $\Delta p = 0$ Pa but only after $\Delta p(t)$ has reached a distinctly positive level, a slower rise of $\Delta p(t)$ directly delays the crossing of this 'critical' level and thus increases t_{det}.

Detachment onset versus time of $\Delta p_{max,Reg}$. To assess whether the onset of detachment is linked to the maximum differential pressure $\Delta p_{Reg,max}$,

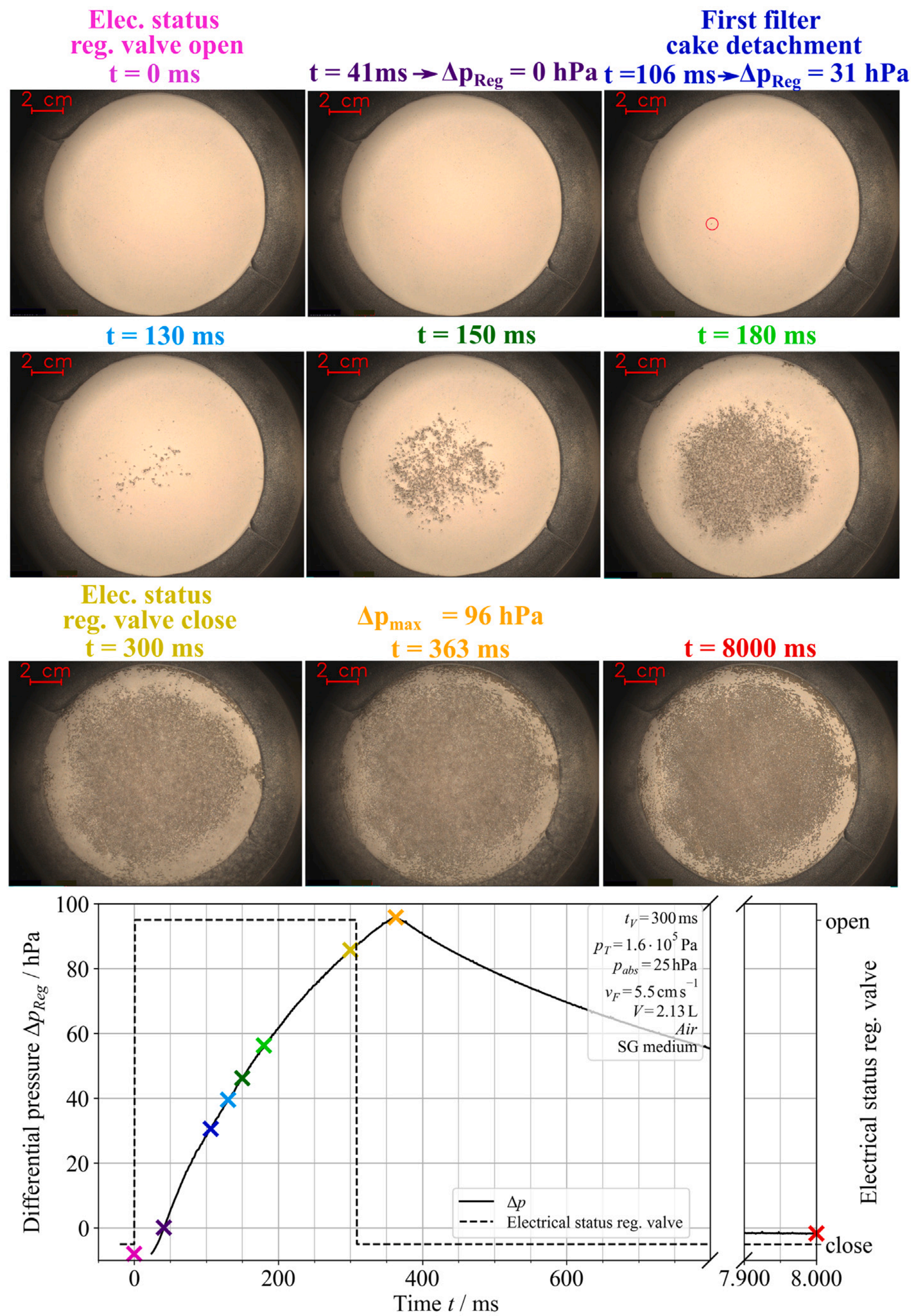

Fig. 13. Selected frame sequence and differential pressure $\Delta p(t)$ for SG filter cake detachment at p_{abs} = 25 hPa, pulse strength high level, t_V = 300 ms, and v_F = 5.5 cm s^{-1}. Presentation as in Fig. 10.

Fig. 15 compares the time of $\Delta p_{max,Reg}$ with the onset time of filter cake detachment t_{det}. For all investigated operating conditions, t_{det} occurs before $\Delta p_{max,Reg}$ is reached (all data points lie above the diagonal), demonstrating that the onset of detachment is not triggered by attaining $\Delta p_{max,Reg}$.

For the SB medium, the data at p_{abs} = 900 hPa are closest to the diagonal, i.e., $\Delta p_{max,Reg}$ is reached comparatively early. With decreasing p_{abs}, t_{det} remains in a similar early time window (on the order of 10 ms), whereas the occurrence of $\Delta p_{max,Reg}$ shifts progressively to later times, reaching several 100 ms at the lowest pressures. This trend is observed for both filter face velocities.

For the SG medium, the first visible detachment occurs earlier for the higher tank pressure (high level) than for the low level. In contrast, the time at which $\Delta p_{max,Reg}$ occurs is largely independent of the pulse strength level at reduced pressures: for p_{abs} < 900 hPa and for both v_F, $\Delta p_{max,Reg}$ is reached at approximately the same time and coincides with the moment at which the regeneration valve closes mechanically.

Detachment onset versus time of $\left(\mathrm{d}\Delta p_{Reg}/\mathrm{d}t\right)_{max}$. Since pulse dynamics are frequently discussed in terms of the maximum differential pressure rise rate $\left(\mathrm{d}\Delta p_{Reg}/\mathrm{d}t\right)_{max}$ (Leubner and Riebel, 2004), Fig. 16 compares the time of $\left(\mathrm{d}\Delta p_{Reg}/\mathrm{d}t\right)_{max}$ with the detachment onset time t_{det} for v_F = 5.5 cm s^{-1} in (a) and v_F = 2 cm s^{-1} in (b). For the SB medium, the data at p_{abs} = 900 hPa down to 25 hPa lie close to the diagonal for both v_F, indicating that detachment starts approximately when $\Delta p(t)$ increases most rapidly. At the lowest pressure (p_{abs} = 10 hPa), the points shift slightly above the diagonal, i.e., $\left(\mathrm{d}\Delta p_{Reg}/\mathrm{d}t\right)_{max}$ is reached marginally after the first visible detachment. A similar small offset is observed at 25 hPa for v_F = 2 cm s^{-1}. This minor deviation may partly arise from the

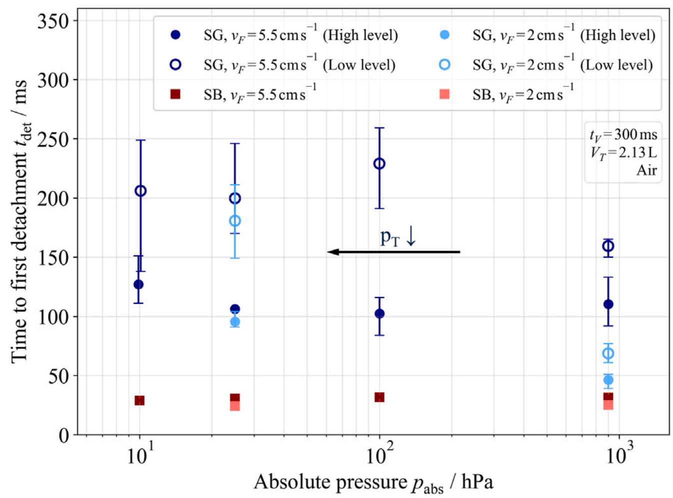

Fig. 14. Time to first visible filter cake detachment t_{det} as a function of absolute pressure p_{abs} at $t_V = 300$ ms. SB: squares. SG: circles (high level filled, low level open). Darker symbols: $v_F = 5.5$ cm s^{-1}; Lighter symbols: $v_F = 2.0$ cm s^{-1}. Error bars indicate minimum/maximum deviation from the mean of three repetitions.

smoothing and binning procedure used to determine $(\mathrm{d}\Delta p_{Reg}/\mathrm{d}t)_{max}$, which is described in detail in Appendix B. Overall, the results support the qualitative picture from the frame sequences: For SB, detachment begins in the very early phase of the pulse and coincides with the onset of flow reversal, which also corresponds to the maximum rise rate of $\Delta p(t)$.

For the SG medium, $(\mathrm{d}\Delta p_{Reg}/\mathrm{d}t)_{max}$ generally occurs before the first visible detachment, i.e., the rapid initial increase of $\Delta p(t)$ alone is not sufficient to initiate filter cake detachment. However, clear and systematic pressure dependencies in t_{RR} are not evident. The 900 hPa cases lie closest to the diagonal, whereas at 25 hPa the maximum rise rate tends to occur earliest. Notably, for $v_F = 2$ cm s^{-1} the times of $(\mathrm{d}\Delta p_{Reg}/\mathrm{d}t)_{max}$ cluster within a narrow range across the SG experiments for both tank pressure levels. Consistent with the comparison to $\Delta p_{max,Reg}$, detachment for SG occurs later in the pulse, i.e., between $(\mathrm{d}\Delta p_{Reg}/\mathrm{d}t)_{max}$ and $\Delta p_{max,Reg}$, consistent with the threshold behavior discussed above.

In summary, SB detachment is governed by the early pulse dynamics near $(\mathrm{d}\Delta p_{Reg}/\mathrm{d}t)_{max}$ and around the flow reversal, whereas SG requires exceeding a positive differential pressure level. These differences are used in the following to interpret the pressure dependence of the cleaning efficiencies.

3.2.3. Cleaning efficiencies E_{opt}, E_{grav} and $E_{\Delta p}$

The regeneration performance is quantified by the optical, gravimetric and differential pressure based cleaning efficiencies, E_{opt}, E_{grav} and $E_{\Delta p}$ (Eqs. (4), (5) and (6)).

Fig. 17 shows the three efficiencies as a function of the absolute pressure p_{abs} for the SB medium, the SG medium at the high pulse strength level, and the SG medium at the low pulse strength level, at $v_F = 5.5$ cm s^{-1}.

Down to 25 hPa the three efficiencies follow the order $E_{\Delta p} \geq E_{opt} \geq E_{grav}$ for all three cases, but the spacing between them differs. For the SB medium E_{grav} lies clearly below E_{opt} and $E_{\Delta p}$, while the efficiencies are high overall. The same order is found for the SG medium at the high level, where the three values lie closer together. For the SG medium at the low level the efficiencies are much lower overall. Here E_{grav} and E_{opt} lie close together, whereas $E_{\Delta p}$ deviates markedly, in particular at 900 hPa. At 10 hPa the order is no longer preserved for the SB medium and for the SG medium at the high level, where $E_{\Delta p}$ falls below E_{opt} and E_{grav}.

The consistent finding $E_{opt} > E_{grav}$ shows that a visually clean surface does not imply complete mass removal. Dust retained in the pore space of the medium and thin residual layers reduce E_{grav}, while they have little effect on E_{opt}. Supportive SEM images are provided in Appendix C (Fig. C.21). E_{grav} also carries a larger experimental uncertainty, because it requires weighing the sample before and after regeneration and therefore an installation and removal step.

Two effects act on $E_{\Delta p}$ in opposite directions. The gas flow after the pulse passes preferentially through the reopened low resistance regions, so that even a partially cleaned surface recovers a large fraction of the cake differential pressure. This raises $E_{\Delta p}$ relative to E_{opt} and E_{grav}. At the same time, dust retained in the medium raises the residual differential pressure and lowers $E_{\Delta p}$. Across the data set $E_{\Delta p}$ exceeds E_{opt} in most cases, which shows that the flow redistribution dominates. The magnitude of this excess is medium dependent. It is small for the SB medium and for the SG medium at the high level, and large for the SG medium at the low level, in particular at 900 hPa.

The reversal at 10 hPa appears for two independent media and only at the lowest absolute pressure, which points to the evaluation of the clean medium differential pressure Δp_{FM} rather than to a medium specific effect. At low absolute pressure Δp_{FM} contributes a large fraction of the total differential pressure and becomes comparable to the cake differential pressure Δp_{FC}, so a small error in Δp_{FM} has a strong effect on $E_{\Delta p}$. In this work Δp_{FM} at operating pressure was estimated by scaling and was not measured for every sample and before every cycle, and the measurements at 900 hPa indicate that the clean medium differential pressure changes over the repeated experiments. This scaling can deviate by up to about 20 % at low absolute pressure (Löschner et al., 2026b). A second explanation cannot be excluded, namely a thin compacted residual layer that is not removed by the pulse and not detected optically, which would keep the residual differential pressure high and lower $E_{\Delta p}$ in the same way. Both effects are consistent with the observed sign and cannot be separated with the present data.

The same measurements were carried out at the lower filter face velocity $v_F = 2.0$ cm s^{-1}. The trends are the same as at $v_F = 5.5$ cm s^{-1}, with higher efficiencies at the lower filter face velocity. The corresponding results are shown in Appendix D (Fig. D.22).

For the subsequent analysis of absolute pressure related flow forces, E_{opt} is used as the primary indicator of cake detachment performance because it directly reflects the spatial removal of cake coverage and captures the characteristic patchiness patterns observed in the high-speed recordings.

To relate cleaning performance to the flow force acting on the cake during the pulse, Fig. 18 shows E_{opt} as a function of the cake related differential pressure contribution during regeneration, $\Delta p_{FC,reg}$, evaluated at operating p_{abs} using Eq. (11). For both media, higher $\Delta p_{FC,reg}$ generally corresponds to higher E_{opt}.

With decreasing p_{abs}, $\Delta p_{FC,reg}$ tends to decrease, and E_{opt} declines accordingly. This effect is substantially more pronounced for SG than for SB. For SG, the high pulse strength level yields larger $\Delta p_{FC,reg}$ and distinctly higher E_{opt} than the low level.

The reduction of $\Delta p_{FC,reg}$ at low p_{abs} can be explained by rarefaction effects, i.e., increasing Knudsen number. Under these conditions, the resistances of cake and filter medium may change differently. Due to the different characteristic pore sizes, the cake resistance can be reduced more strongly with decreasing p_{abs} than the medium resistance, which shifts the partitioning of $\Delta p_{max,Reg}$ such that a smaller fraction is available across the cake (cf. Section 2.4.4). In addition, the reduced gas density lowers the transient mass flux and jet momentum for a given pressure level, further weakening the effective mechanical forcing on the cake.

Beyond these flow related effects, the flexibility of the SB medium provides an additional detachment contribution via deformation induced acceleration forces (see Introduction), which is absent for the rigid SG medium. This helps explain why SG can exhibit substantially

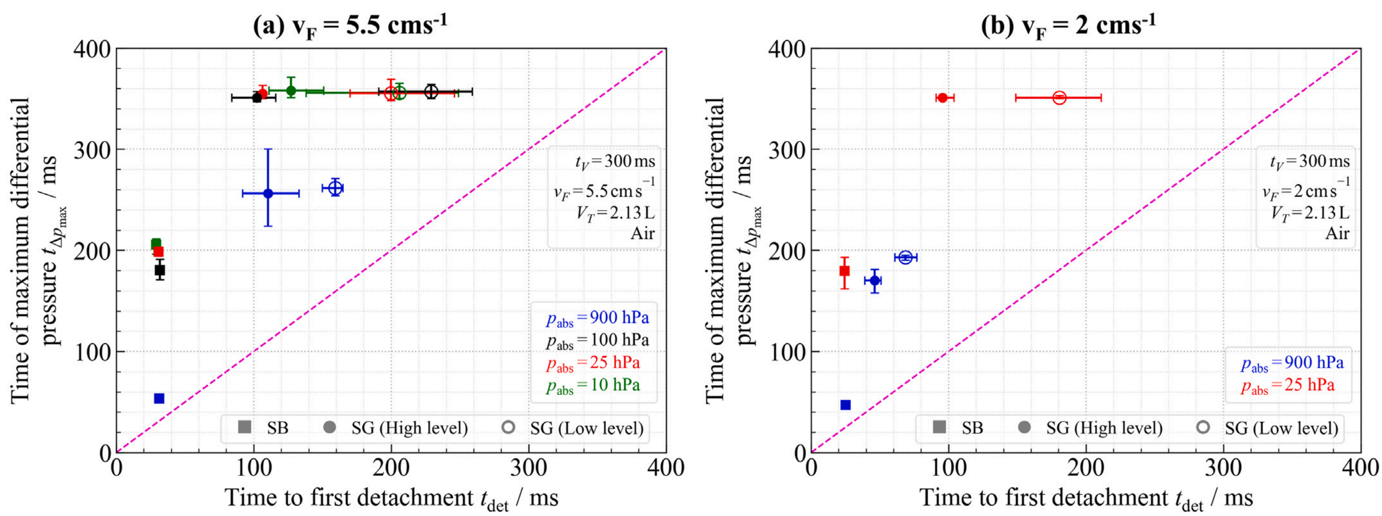

Fig. 15. Time of maximum differential pressure $\Delta p_{Reg,\max}$ plotted against the time to first visible detachment t_{det} for (a) $v_F = 5.5\,\text{cm}\,\text{s}^{-1}$ and (b) $v_F = 2.0\,\text{cm}\,\text{s}^{-1}$ at $t_V = 300\,\text{ms}$. Colors indicate p_{abs}. SB: squares. SG: circles (high level filled, low level open). The dashed diagonal marks equality of both times.

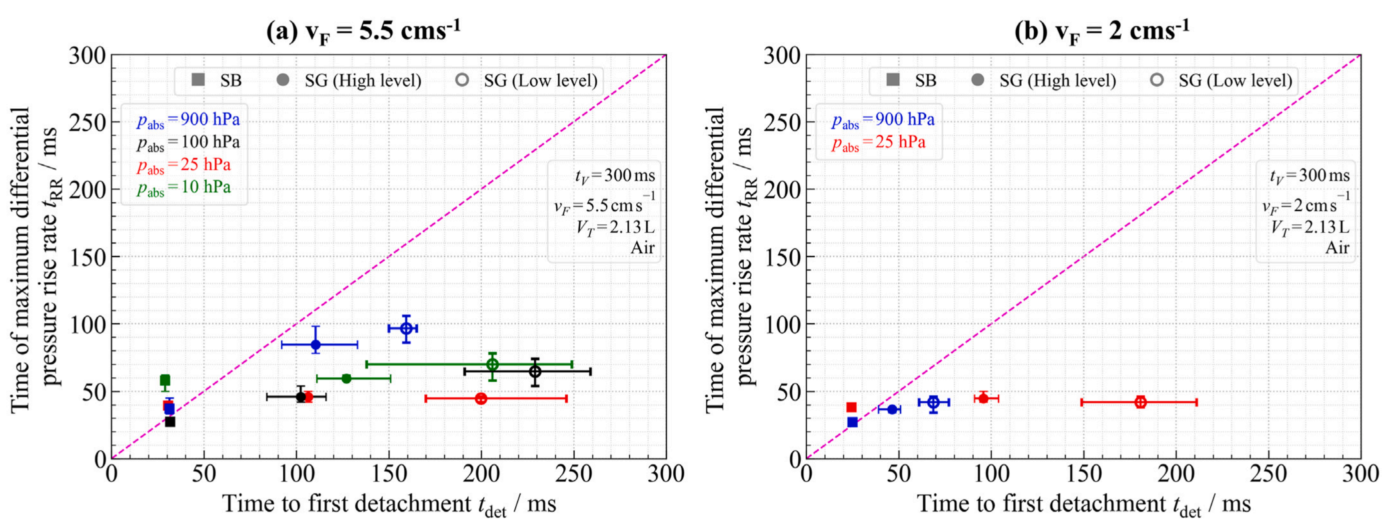

Fig. 16. Time of maximum differential pressure rise rate $(\mathrm{d}\Delta p_{\text{Reg}}/\mathrm{d}t)_{\max}$ plotted against the time to first visible detachment t_{det} for (a) $v_F = 5.5\,\text{cm}\,\text{s}^{-1}$ and (b) $v_F = 2.0\,\text{cm}\,\text{s}^{-1}$ at $t_V = 300\,\text{ms}$. Colors indicate p_{abs}. SB: squares. SG: circles (high level filled, low level open).

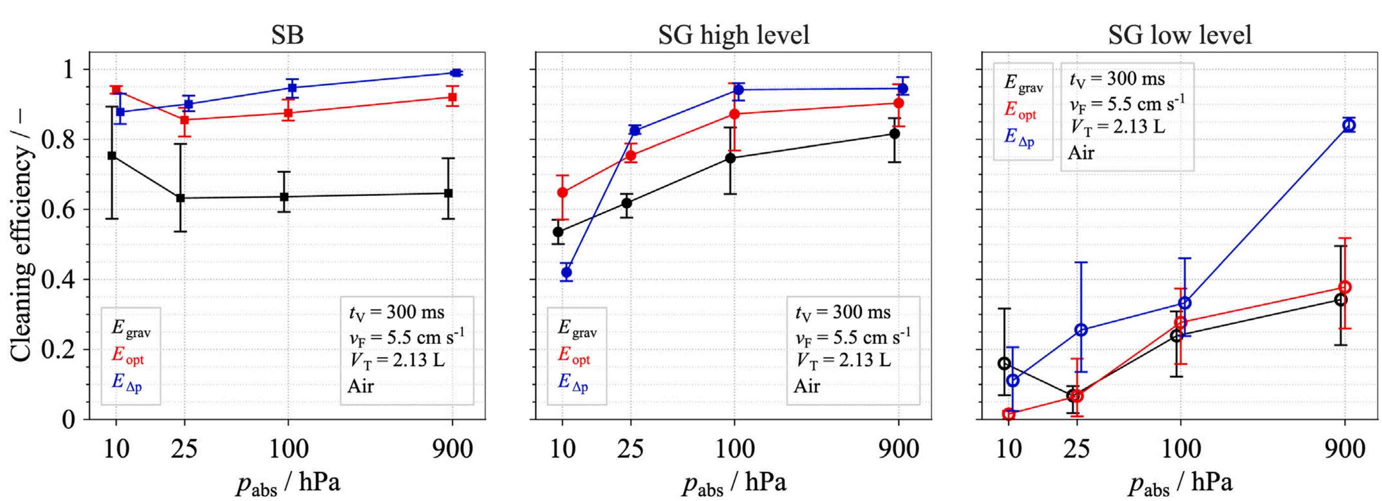

Fig. 17. Cleaning efficiencies E_{grav} (black), E_{opt} (red) and $E_{\Delta p}$ (blue) as a function of absolute pressure p_{abs} for the SB medium, the SG medium at high pulse strength level, and the SG medium at low pulse strength level at $v_F = 5.5\,\text{cm}\,\text{s}^{-1}$ and $t_V = 300\,\text{ms}$. Symbols represent mean values of three repetitions; error bars indicate minimum/maximum deviation from the mean.

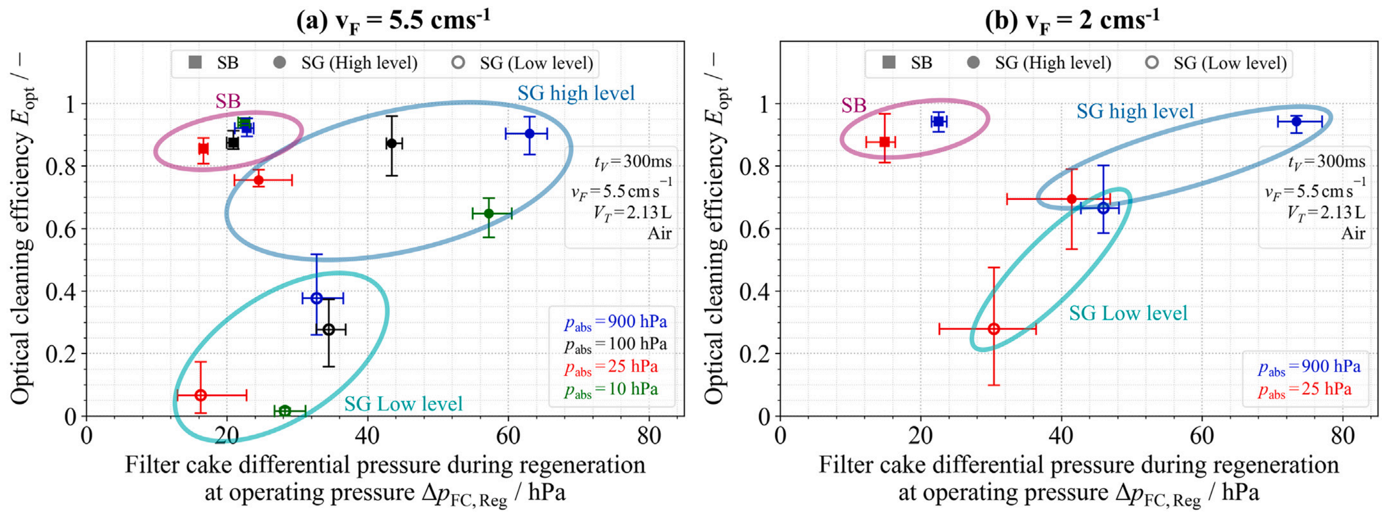

Fig. 18. Mean optical cleaning efficiency E_{opt} as a function of the cake related differential pressure contribution during regeneration at operating conditions, $\Delta p_{FC,reg}$, for (a) $v_F = 5.5\,\mathrm{cm\,s^{-1}}$ and (b) $v_F = 2.0\,\mathrm{cm\,s^{-1}}$ at $t_V = 300\,\mathrm{ms}$. Squares: SB medium. Circles: SG medium (high level filled, low level open). Colors indicate p_{abs}. Symbols represent mean values of three repetitions; error bars indicate minimum/maximum deviation from the mean.

lower E_{opt} than SB even when comparable $\Delta p_{FC,reg}$ values are reached (notably for SG high level).

Deviations from the overall trends can be attributed to experimental constraints and sample specific effects. For SB at 10 hPa, the elevated $\Delta p_{FC,reg}$ and the comparatively high E_{opt} reflect the higher than intended pulse strength (Section 3.1). For SG, the 10 hPa experiments were conducted with different samples than at higher pressures. Therefore, the 10 hPa SG point should not be interpreted as a purely pressure induced effect. Overall, the data indicate that the decline in E_{opt} with decreasing p_{abs} is consistent with a reduced $\Delta p_{FC,reg}$ at operating conditions, while medium flexibility (SB) provides an additional detachment mechanism that mitigates this effect compared to the rigid SG medium.

4. Conclusions and outlook

Valve opening time t_V primarily affects pulse duration, while $\Delta p_{max,Reg}$ is nearly independent of t_V for the SB medium within the investigated range. For the SG medium, sufficiently long t_V is required to fully develop $\Delta p_{max,Reg}$, consistent with its higher flow resistance. At constant p_T, lowering p_{abs} increases p_T/p_{abs}, which leads to higher $\Delta p_{max,Reg}$ and a delayed occurrence of the maximum. Therefore, p_T must be adjusted when varying p_{abs} to reach comparable target pulse strengths.

High-speed imaging shows that cake detachment for the SB medium starts essentially at flow reversal ($\Delta p \approx 0$) and is completed well before $\Delta p_{max,Reg}$ occurs. In contrast, SG requires a significant positive differential pressure level for onset, resulting in delayed detachment and a stronger dependence on p_{abs} and pulse strength level. Quantitatively, the SB detachment onset time t_{det} aligns closely with the time of $(\mathrm{d}\Delta p_{Reg}/\mathrm{d}t)_{max}$, indicating that pulse dynamics early in the regeneration process govern initial release. For SG, $(\mathrm{d}\Delta p_{Reg}/\mathrm{d}t)_{max}$ occurs well before t_{det}, and detachment onset takes place between $(\mathrm{d}\Delta p_{Reg}/\mathrm{d}t)_{max}$ and $\Delta p_{max,Reg}$. For both media, $\Delta p_{max,Reg}$ is reached after the first visible detachment. Overall, these findings show that the detachment onset is governed by different pulse characteristics ($\Delta p_{Reg,max}$ and $(\mathrm{d}\Delta p_{Reg}/\mathrm{d}t)_{max}$) depending on the mechanical properties of the filter medium (thickness, porosity, …) and its flow resistance.

The optical, gravimetric and differential pressure based efficiencies E_{opt}, E_{grav} and $E_{\Delta p}$ all decrease with decreasing p_{abs} when pulse strength is kept comparable, with a stronger sensitivity for SG than for SB. SG shows a pronounced dependence on pulse strength level, where the high level is required to maintain high efficiencies at reduced absolute pressure. Down to 25 hPa the three efficiencies follow the order $E_{\Delta p} \geq E_{opt} \geq E_{grav}$. The frequent observation $E_{opt} > E_{grav}$ is attributed to residual dust in the filter structure and thin remaining layers (Section 3.2.3). $E_{\Delta p}$ is the highest of the three because the restored gas flow passes preferentially through the reopened low resistance regions. This excess is small for the SB medium and the SG high level and large for the SG low level. At 10 hPa the order reverses for the SB medium and the SG high level, which is attributed to the strong influence of the clean medium differential pressure on $E_{\Delta p}$ at low absolute pressure. Lowering the filter face velocity improves regeneration. The reduction in cleaning efficiency at low p_{abs} correlates with a decrease of the cake related differential pressure contribution $\Delta p_{FC,reg}$, indicating weaker effective forces due to resistance partitioning under rarefied conditions and reduced gas density. Setup constraints (SB at 10 hPa) and sample changes (SG at 10 hPa) must be considered when interpreting the lowest pressure points.

Future work could aim at developing a predictive model for the transient pressure pulse during regeneration. Such a model would allow the experimentally observed $\Delta p(t)$ characteristics at reduced p_{abs} to be reproduced and parameterized, and it could support the design of comparable pulse conditions across operating pressures.

In addition, it would be valuable to investigate pure backflushing (flow reversal without a pronounced pressure pulse) to isolate the contribution of flow reversal from pulse induced momentum and pressure wave effects. Moreover, multiple consecutive regeneration cycles should be performed at fixed operating points to quantify the influence of p_{abs} on long term behavior, for example cumulative dust penetration, residual layer build-up, and filter aging effects. From an optical diagnostics perspective, a second high-speed camera oriented perpendicular to the filter surface could provide complementary information on filter medium motion and particle trajectories during detachment. Furthermore, the influence of the mass loading on the filter medium should be investigated, and the sensitivity of the observed trends to the choice of test dust should be assessed by varying the dust material and its size distribution. For a more robust differential pressure based evaluation at low absolute pressure, the clean medium differential pressure Δp_{FM} should be measured for each sample and before each regeneration cycle rather than estimated by scaling. Furthermore, the flow field during pulse injection at reduced absolute pressure, including the jet development and the pressure wave propagation toward the filter medium, could not be characterized in this work and should be addressed in future studies.

CRediT authorship contribution statement

Vanessa Löschner: Writing – original draft, Visualization, Validation, Software, Project administration, Methodology, Investigation, Formal analysis, Data curation. **Patricia Heuer:** Writing – review & editing, Visualization, Investigation. **Jörg Meyer:** Writing – review & editing, Methodology, Formal analysis, Conceptualization. **Achim Dittler:** Writing – review & editing, Supervision, Resources, Funding acquisition, Conceptualization.

Declaration of Generative AI and AI-assisted technologies in the writing process

During the preparation of this manuscript, the authors used Claude (Anthropic) and ChatGPT (OpenAI) to improve language clarity and readability. All scientific content, interpretations and conclusions were produced and verified by the authors. The authors take full responsibility for the accuracy and integrity of the work.

Funding statement

This research was funded by the Deutsche Forschungsgemeinschaft (DFG, German Research Foundation), grant number: 541566488.

Declaration of competing interest

The authors declare that they have no known competing financial interests or personal relationships that could have appeared to influence the work reported in this paper.

Acknowledgments

We gratefully acknowledge that this project was funded by the Deutsche Forschungsgemeinschaft (DFG, German Research Foundation) – 541566488.

We acknowledge the collaboration of Herding GmbH Filtertechnik for providing the SG medium and Freudenberg Filtration Technologies GmbH & Co. KG for providing the SB medium used in this work.

Appendix A. Influence of valve opening time on the differential pressure behavior during regeneration of clean filter media

As a first step, the influence of the valve opening time t_V on the pulse shape and strength is examined in order to verify the commonly reported observation that t_V has only a minor effect on the maximum differential pressure during the pulse within typical operating ranges (Leubner and Riebel, 2004). This initial analysis is performed to select a sufficiently long t_V that ensures fully developed pulse formation and provides a consistent reference setting for the subsequent investigation of the remaining operating parameters. Fig. A.19 shows the differential pressure during regeneration for the SB medium (Fig. A.19a) and the SG medium (Fig. A.19b); operating conditions and presentation are given in the caption. All differential pressure profiles are presented such that the electric valve opening time is set to $t = 0$. Note that the vertical axis scaling differs between (a) and (b).

All regeneration traces are plotted from the time when the measured differential pressure exceeds the lower limit of the high resolution sensor of approximately −8 hPa (Section 2.1.1). This is a plotting convention imposed by the sensor range and does not indicate a physical onset of regeneration.

For the SB medium, $\Delta p_{\mathrm{max,Reg}}$ remains essentially unchanged across all tested valve opening times. Moreover, the time at which $\Delta p_{\mathrm{max,Reg}}$ occurs is approximately the same for all t_V, whereas the pulse duration increases with increasing t_V. This is consistent with (Leubner and Riebel, 2004). The measurements also reveal time delays between the electrical trigger of the regeneration valve and the mechanical valve motion. The onset of the differential pressure rise occurs about 20 ms after the electrical opening signal, and the effective mechanical closing lags the electrical closing signal by roughly 50 ms, which is visible as a distinct kink in the $\Delta p(t)$ trace.

Superimposed oscillations are observed for the SB medium. Rothwell et al. reported that pressure fluctuations superimposed on the main overpressure pulse are an inherent feature of the jet-injector assembly and should be interpreted as irregular turbulent pressure pulses superimposed on a more slowly varying pressure continuum rather than as a purely periodic oscillation (Rothwell, 1991b,a). Concerning their physical origin, (Rothwell, 1991a) (as cited by Leubner and Riebel, 2004) suggested that such oscillations may arise from reflections of pressure waves at the walls of the filter housing. (Leubner and Riebel, 2004), however, argue that the oscillations are too regular and too high in frequency for a purely reflection driven mechanism and showed, based on local dynamic pressure measurements, that they originate in the injector system, i.e., at the location where compressed air is discharged, and are subsequently transmitted into the filter assembly. They further reported a strong dependence on the measurement location and attenuation by both filter elements and filter cakes, while a clear correlation with cleaning performance could not be established (Leubner and Riebel, 2004).

For the SG medium, the transient differential pressure behavior differs from that of the SB medium with respect to the time required to reach the maximum differential pressure $\Delta p_{\mathrm{max,Reg}}$. Increasing the valve opening time from $t_V = 100\,\mathrm{ms}$ to $200\,\mathrm{ms}$ systematically increases $\Delta p_{\mathrm{max,Reg}}$. Further increases in t_V do not increase $\Delta p_{\mathrm{max,Reg}}$ any further (Fig. A.19b). A plausible explanation is the considerably higher flow resistance of the SG medium, which alters the transient pressurization and flow reversal during the pulse and thereby delays the development of $\Delta p_{\mathrm{max,Reg}}$ compared to the more permeable SB medium. Additionally, weak superimposed oscillations are also present for the SG medium. However, they appear less pronounced in Fig. A.19b because the larger Δp levels require a different axis scaling.

Based on these results, a valve opening time of $t_V = 300\,\mathrm{ms}$ is selected for all subsequent experiments. This ensures that $\Delta p_{\mathrm{max,Reg}}$ has reached its plateau for the SG medium and, for consistency and comparability, the same t_V is also used for the SB medium.

Appendix B. Procedure for determining the maximum differential pressure rise rate

To quantify the pulse dynamics, the maximum differential pressure rise rate $\left(\mathrm{d}\Delta p_{\mathrm{Reg}}/\mathrm{d}t\right)_{\max}$ and the corresponding time $t_{RR,\max}$ are determined from the measured differential pressure signal $\Delta p_{\mathrm{Reg}}(t)$ during regeneration. Fig. B.20 shows two representative examples at $p_{\mathrm{abs}} = 900\,\mathrm{hPa}$ for the SB medium (Fig. B.20a) and the SG medium (Fig. B.20c). Raw data are shown in black. The dashed curve indicates the electrical valve signal, where $t = 0$ is defined as the onset of the electrical opening signal.

Prior to differentiation, $\Delta p_{\mathrm{Reg}}(t)$ is smoothed by fixed time binning to suppress oscillations and to obtain a robust estimate of the rise rate. The signal is divided into non-overlapping time windows of width Δt_{bin} and the mean value within each window is computed. For the SB medium at $p_{\mathrm{abs}} = 900\,\mathrm{hPa}$, pronounced oscillations are superimposed on the differential pressure. Therefore, $\Delta t_{\mathrm{bin}} = 6\,\mathrm{ms}$ is used for all SB data at $p_{\mathrm{abs}} = 900\,\mathrm{hPa}$. For all other cases, including SG and SB at reduced absolute pressure, the signals are considerably smoother and $\Delta t_{\mathrm{bin}} = 4\,\mathrm{ms}$ is applied. The resulting binned curves are shown in red in Fig. B.20a and B.20c.

The rise rate is computed from the binned mean values $\overline{\Delta p_i}$ using a first-difference scheme

$$\left(\frac{\mathrm{d}\Delta p_{\mathrm{Reg}}}{\mathrm{d}t}\right)_i \approx \frac{\overline{\Delta p_{i+1}} - \overline{\Delta p_i}}{\Delta t_{\mathrm{bin}}},$$

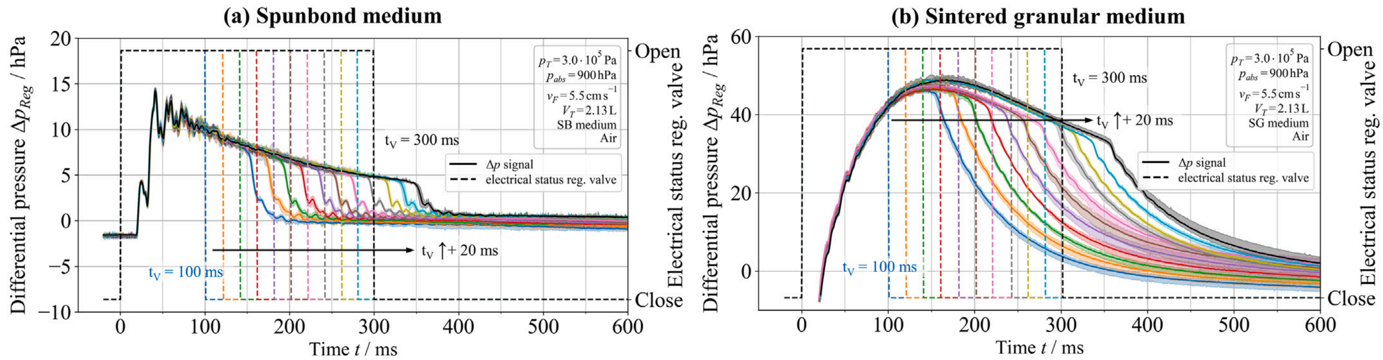

Fig. A.19. Differential pressure $\Delta p(t)$ during regeneration for varying valve opening time t_V at $p_{\mathrm{abs}} = 900\,\mathrm{hPa}$, $p_T = 3 \cdot 10^5\,\mathrm{Pa}$, and $v_F = 5.5\,\mathrm{cm\,s^{-1}}$ in air: (a) SB medium and (b) SG medium. t_V is increased from 100 ms to 300 ms in 20 ms steps; each curve is the mean of five pulses and the band indicates minimum/maximum deviation. Solid lines show $\Delta p(t)$; dashed lines indicate the electrical valve signal.

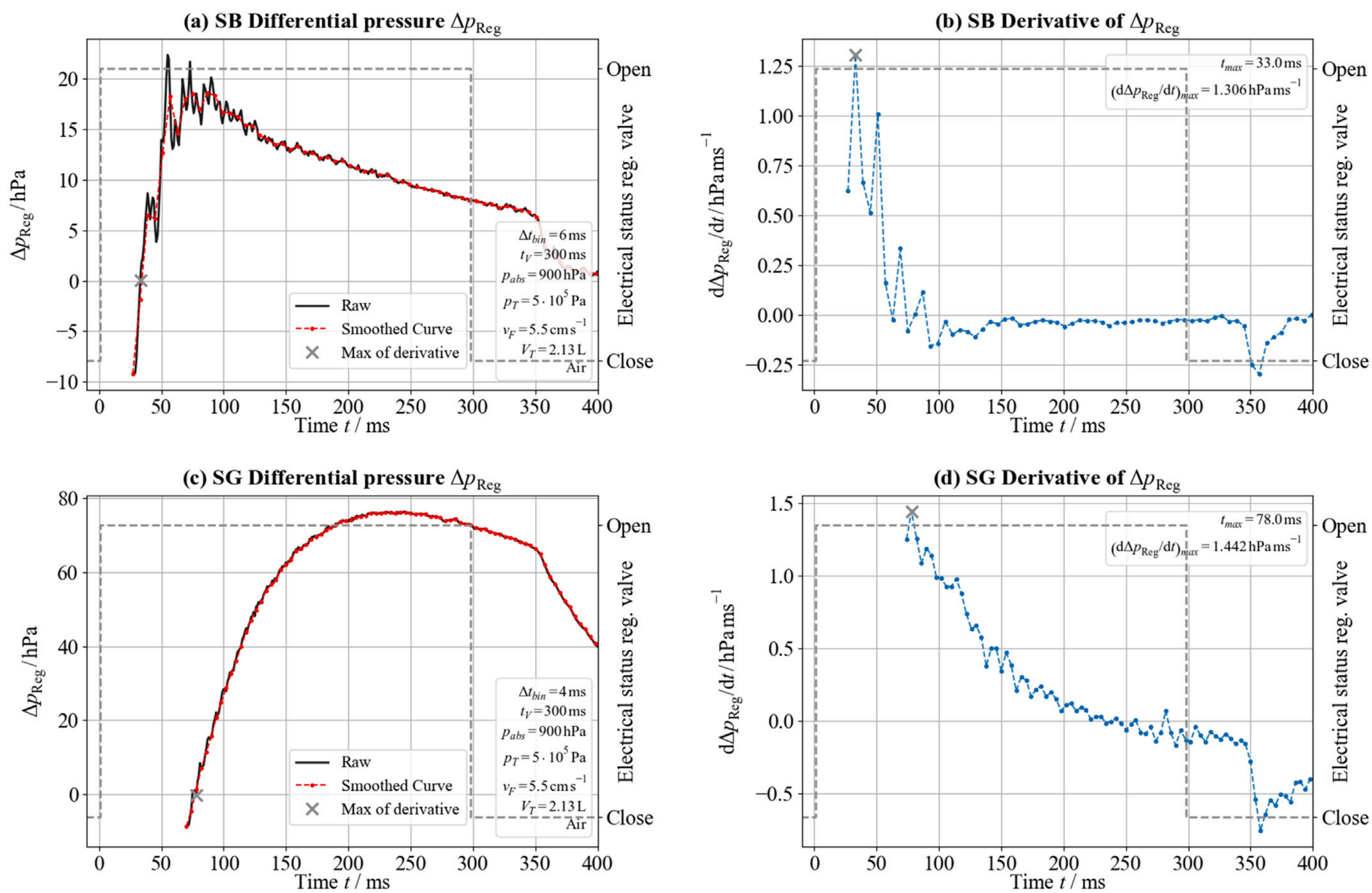

Fig. B.20. Determination of the maximum differential pressure rise rate $(\mathrm{d}\Delta p_{\mathrm{Reg}}/\mathrm{d}t)_{\max}$ and its time $t_{RR,max}$ from the regeneration differential pressure signal. (a,c) Raw data (black) and time-binned smoothed curves (red) for SB and SG; (b,d) derivative of the smoothed curves. The electrical valve signal is shown as dashed line.

and the corresponding time is assigned to the midpoint of the respective interval. Fig. B.20b and B.20d show the resulting derivatives for SB and SG.

The maximum of the derivative yields $(\mathrm{d}\Delta p_{\mathrm{Reg}}/\mathrm{d}t)_{\max}$ and its time coordinate defines $t_{RR,\max}$. The rise rate is evaluated over the measurable range down to −8 hPa (Section 2.1.1); extrema at more negative values cannot be resolved and are not considered, since detachment is governed by the subsequent positive differential pressure. In all panels, the identified maximum rise rate is marked by a gray marker. The same time instant is highlighted in the corresponding $\Delta p_{\mathrm{Reg}}(t)$ curves in Fig. B.20a and B.20c to enable a direct visual association between pressure signal and rise-rate maximum.

Appendix C. SEM images of regenerated SB medium

Fig. C.21 shows exemplary SEM images of the SB medium after regeneration, recorded at the locations indicated on the filter sample (right). Although large parts of the surface can appear optically clean after pulsing, fine dust particles are still visible on the fibers and within the porous structure, and residual deposits can be found both in the interior (cross-section) and locally as thicker patches on the upstream

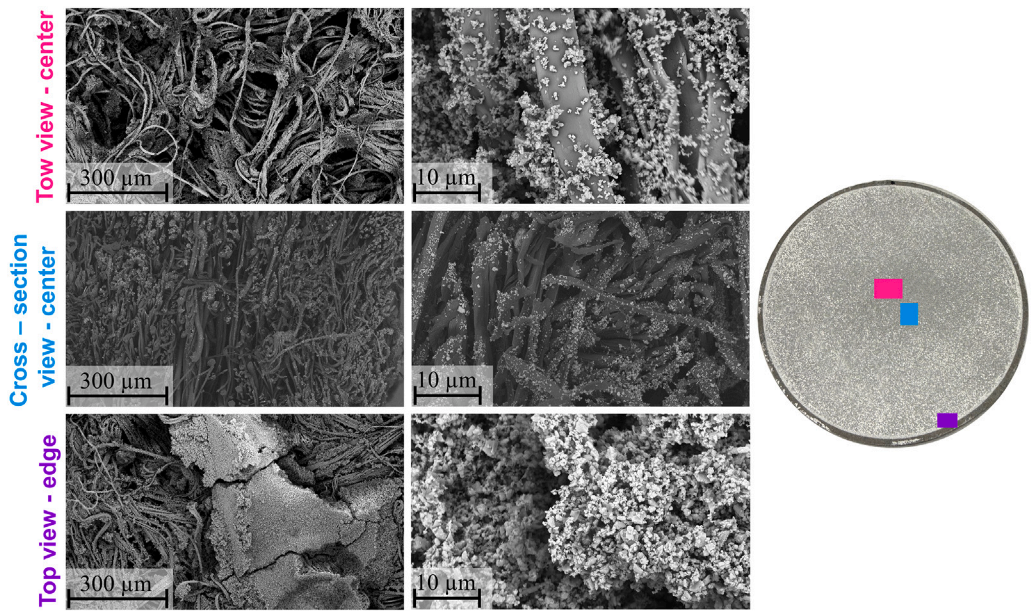

Fig. C.21. Exemplary SEM images of the regenerated SB medium. Rows: top view at the center, cross-section at the center, and top view near the edge; each row shows an overview image (first column) and a higher magnification detail (second column). The sample locations are marked on the filter coupon (right).

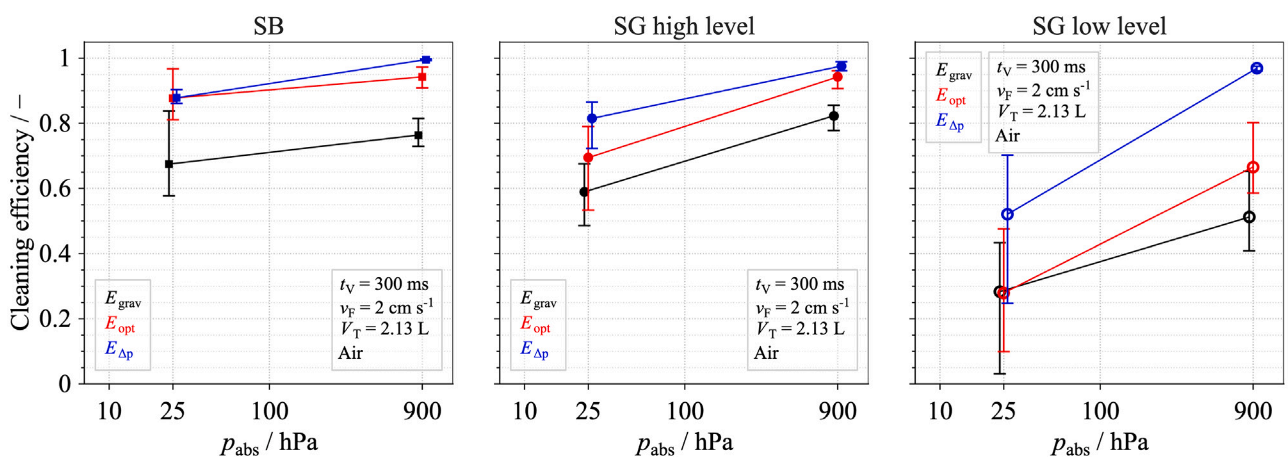

Fig. D.22. Cleaning efficiencies E_{grav} (black), E_{opt} (red) and $E_{\Delta p}$ (blue) as a function of absolute pressure p_{abs} at $v_F = 2.0\,\text{cm}\,\text{s}^{-1}$ and $t_V = 300\,\text{ms}$ for the SB medium, the SG medium at high pulse strength level, and the SG medium at low pulse strength level.

media surface, particularly towards the edge. This is consistent with the discussion of $E_{\text{opt}} > E_{\text{grav}}$ in Section 3.2.3.

Appendix D. Cleaning efficiencies at reduced filter face velocity

Fig. D.22 shows the cleaning efficiencies E_{grav}, E_{opt} and $E_{\Delta p}$ as a function of p_{abs} at $v_F = 2.0\,\text{cm}\,\text{s}^{-1}$. The trends are the same as at $v_F = 5.5\,\text{cm}\,\text{s}^{-1}$, with higher efficiencies at the lower filter face velocity.

Appendix E. Supplementary data

Supplementary material related to this article can be found online at https://doi.org/10.1016/j.cherd.2026.08.058.

References

Amjad, A.I., 2022. Filtration in pharmaceutical industries and role of textile. TEKS 65 (3), 227–241. http://dx.doi.org/10.14502/tekstilec.65.2022036.

Bächler, P., Meyer, J., Dittler, A., 2023. Operating Behavior of Pulse Jet-Cleaned Filters Regarding Energy Demand and Particle Emissions – Part 1: Experimental Parameter Study. Chem Eng & Technol 46 (8), 1689–1697. http://dx.doi.org/10.1002/ceat.202300080.

Bächler, P., Meyer, J., Dittler, A., 2026. Implications for the energy-evaluation of pulse-jet cleaned surface filter media regarding filter operation during typical test procedures. Powder Technol. 469, 121889. http://dx.doi.org/10.1016/j.powtec.2025.121889.

Beuth Verlag, 2010. VDI 3677 Blatt 1:2023-05, Filternde Abscheider - Oberflächenfilter.

Binnig, J., Bredin, A., Meyer, J., Kasper, G., 2011. Dimensional analysis of the cleaning pulse intensity in a surface filter test rig. Powder Technol. 211 (2–3), 275–279. http://dx.doi.org/10.1016/j.powtec.2011.04.037.

Brown, R.C., 2001. Filtration in Industrial Hygiene. AIHAJ - Am. Ind. Hyg. Assoc. 62 (5), 633–643. http://dx.doi.org/10.1080/15298660108984663.

Dittler, A., 2001. Gasreinigung mit starren Oberflächenfiltern - Erscheinungsformen und Auswirkungen unvollständiger Filterregenerierung. In: Berichte aus der Verfahrenstechnik, Shaker, Aachen.

Hasler, P., Nussbaumer, T., 1999. Gas cleaning for IC engine applications from fixed bed biomass gasification. Biomass Bioenergy 16 (6), 385–395. http://dx.doi.org/10.1016/S0961-9534(99)00018-5.

Jorisch, W., 1999. Vakuumtechnik: in der Chemischen Industrie. Wiley-VCH, Weinheim, OCLC: 85820458.

Jousten, 2018. Handbuch Vakuumtechnik. Springer Fachmedien Wiesbaden, OCLC: 1105115344.

Klingel, R., Löffler, F., 1984. Zur Frage der optimalen Reinigungsbedingungen für Schlauchfilter mit Druckstossabreinigung. Chem. Eng. Process.: Process. Intensif. 18 (4), 189–198. http://dx.doi.org/10.1016/0255-2701(84)87002-6.

Koch, D., Seville, J., Clift, R., 1996. Dust cake detachment from gas filters. Powder Technol. 86 (1), 21–29. http://dx.doi.org/10.1016/0032-5910(95)03033-6.

Krammer, G., Holzinger, F., 2022. Movement of flexible filter media under pulse-jet filter cleaning conditions. Chem. Eng. Res. Des. 188, 1054–1066. http://dx.doi.org/10.1016/j.cherd.2022.11.002.

Kurtz, O., Meyer, J., Kasper, G., 2016. Influence of filter operating parameters on fine dust emissions from pulse-cleaned filter bags. Chem Eng & Technol 39 (3), 435–443. http://dx.doi.org/10.1002/ceat.201500340.

Leubner, H., Riebel, U., 2003. Druckstoß abreinigung textiler und starrer Filtermedien: Abreinigungsrelevante Parameter. Chem. Ing. Tech. 75 (5), 504–514. http://dx.doi.org/10.1002/cite.200390099.

Leubner, H., Riebel, U., 2004. Pulse jet cleaning of textile and rigid filter media – characteristic parameters. Chem Eng & Technol 27 (6), 652–661. http://dx.doi.org/10.1002/ceat.200406129.

Liu, X., Shen, H., 2019. Effect of Venturi Structures on the Cleaning Performance of a Pulse Jet Baghouse. Appl. Sci. 9 (18), 3687. http://dx.doi.org/10.3390/app9183687.

Löffler, F., 1988. Staubabscheiden. In: Lehrbuchreihe Chemieingenieurwesen/Verfahrenstechnik, vol. 4, Thieme, Stuttgart and New York.

Löffler, F., Dietrich, H., Flatt, W., 1984. Staubabscheidung mit Schlauchfiltern und Taschenfiltern. Vieweg, Braunschweig, OCLC: 500079939.

Löschner, V., Lüttmann, J., Meyer, J., Dittler, A., 2026a. Dust cake build-up on gas cleaning surface filters at ambient and low absolute pressure. Sep. Purif. Technol. 381, 135536. http://dx.doi.org/10.1016/j.seppur.2025.135536.

Löschner, V., Meyer, J., Dittler, A., 2025. Experimental and theoretical investigation of the pressure drop across different surface filter media at low absolute pressures down to 100 Pa. Sep. Purif. Technol. 361, 131093. http://dx.doi.org/10.1016/j.seppur.2024.131093.

Löschner, V., Meyer, J., Dittler, A., 2026b. Dust cake pressure drop determination of surface filters at low absolute pressures. Chem. Eng. Technol. 49 (5), e70226. http://dx.doi.org/10.1002/ceat.70226.

Otsu, N., 1979. A threshold selection method from gray-level Histograms. IEEE Trans. Syst. Man Cybern. 9 (1), 62–66. http://dx.doi.org/10.1109/TSMC.1979.4310076.

Rothwell, E., 1991a. Pulse-jet driven injectors for fabric dust filters: (Part 1) The significance of jet-injector interaction. Filtr. Sep. 28 (5), 341–350. http://dx.doi.org/10.1016/0015-1882(91)80158-2.

Rothwell, E., 1991b. Pulse-jet injectors for fabric dust filters: (Part 2) The fine structure of the overpressure pulse. Filtr. + Sep. 28 (6), 420–426. http://dx.doi.org/10.1016/0015-1882(91)80265-7.

Schmidt, E., 1998. Abscheidung von Partikeln aus Gasen mit Oberflachenfiltern. VDI Verlag, Dusseldorf, OCLC: 45561735.

Schuberth, J., Mauschitz, G., Höflinger, W., 2011. Clogging mechanisms involved in the aging process of cleanable filter media. Sep. Purif. Technol. 77 (2), 196–201. http://dx.doi.org/10.1016/j.seppur.2010.12.004.

Sievert, J., Löffler, F., 1989. Fabric cleaning in pulse-jet filters. Chem. Eng. Process.: Process. Intensif. 26 (2), 179–183. http://dx.doi.org/10.1016/0255-2701(89)90010-X.

Silva, C., Negrini, V., Aguiar, M., Coury, J., 1999. Influence of gas velocity on cake formation and detachment. Powder Technol. 101 (2), 165–172. http://dx.doi.org/10.1016/S0032-5910(98)00168-5.

Simon, X., Chazelet, S., Thomas, D., Bémer, D., Régnier, R., 2007. Experimental study of pulse-jet cleaning of bag filters supported by rigid rings. Powder Technol. 172 (2), 67–81. http://dx.doi.org/10.1016/j.powtec.2006.10.005.

Thier, B. (Ed.), 1997. Apparate Technik - Bau - Anwendung, 2. Ausg Vulkan-Verl, Essen, OCLC: 75851114.

Van'T Land, C.M., 2011. Drying in the Process Industry, first ed. Wiley, http://dx.doi.org/10.1002/9781118105818.

Verein Deutscher Ingenieure e.V., 2014. Prüfung von Filtermedien für Abreinigungsfilter: Standardprüfung zur vergleichenden Bewertung von. Issue: VDI 3926 Blatt 1 Place: Berlin Volume: 13.040.10.

Wines, T.H., Mokhatab, S., 2022. Contamination Control in the Natural Gas Industry. Gulf Professional Publishing, Cambridge, MA, OCLC: 1286498889.

Yu, Z., Muraoka, Y., Furumoto, K., Fukasawa, T., Ishigami, T., Liu, J., Fukui, K., 2024. A novel pulse-jet cleaning method to effectively extend the lifetime of pleated filter and reduce dust emission. Adv. Powder Technol. 35 (5), 104456. http://dx.doi.org/10.1016/j.apt.2024.104456.